AMAS COURSE ON MECHANICS OF ADVANCED MATERIALS
MAM'2001 – (PP.43–84) – WARSAW, OCTOBER 8-12, 2001.

Deformation mechanisms in TiAl intermetallics – experiments and modelling

F.D. FISCHER

Institute of Mechanics
Montanuniversitaet Leoben
Franz-Josef-Strasse 18, A-8700 Leoben, Austria
e-mail: fischer@unileoben.ac.at

The mechanical properties of intermetallic γ-TiAl based materials depend strongly on the microstructure, which in turn is influenced by the alloy chemistry and the applied heat treatment. First, a computational study of the room temperature deformation behavior of γ-TiAl based two-phase alloys exhibiting a globular near-γ microstructure is presented. The micromechanical model is based on the unit-cell technique using the finite element method. In the applied crystal plasticity concept crystallographic slip and deformation twinning are taken into account as the dominant deformation mechanisms. The conclusions drawn from the simulations are discussed and compared to experimental results obtained from acoustic emission measurements and transmission electron microscopy investigations. Furthermore, the creep behavior of a designed fully lamellar (DFL) γ-TiAl microstructure is investigated. Differently spaced DFL microstructures were adjusted in order to investigate their influence on creep. The interface spacing was varied in the range of 1.2 μm to 0.14 μm by altering the cooling rates from 1 K/min to 200 K/min, and short term creep tests were carried out in air under various temperature/load conditions. A first approach in modelling the steady state creep deformation of the fully lamellar material in question is presented. A power law description for diffusion controlled dislocation creep is proposed, and a structure factor is introduced which depends on the lamellar orientation with respect to the loading axis as well as on the mean lamellar interface spacing.

Key words: *γ-TiAl, micromechanical modelling, crystal plasticity, acoustic emission, twinning, creep.*

1. Introduction

1.1. What are intermetallics

The author of this paper takes the liberty of explaining "intermetallics" from the point of view of a mechanical engineer. Therefore, metal physicists and physicochemists are humbly asked to apologize the "crude" and (probably unprecise) definition. In our definition, intermetallics are stoichiometric compositions of metals. As generally accepted, metallic alloys, hence also intermetallics, form a crystal microstructure with grains being individual crystals. Considering such a crystal e.g. two different metals forming the crystal occupy different lattice positions. From here on we will concentrate on TiAl intermetallics. A prominent representative, γ-TiAl,

forms a face centered cubic (i.e. slightly tetragonal) lattice with "unit cubes" having Al-atoms in the top and bottom side surfaces and Ti-atoms in the middles of the remaining four side surfaces. To explain the variety of TiAl intermetallics, a phase diagram is depicted in Fig. 1 showing the various chemical and crystallographic variants of this type of intermetallics.

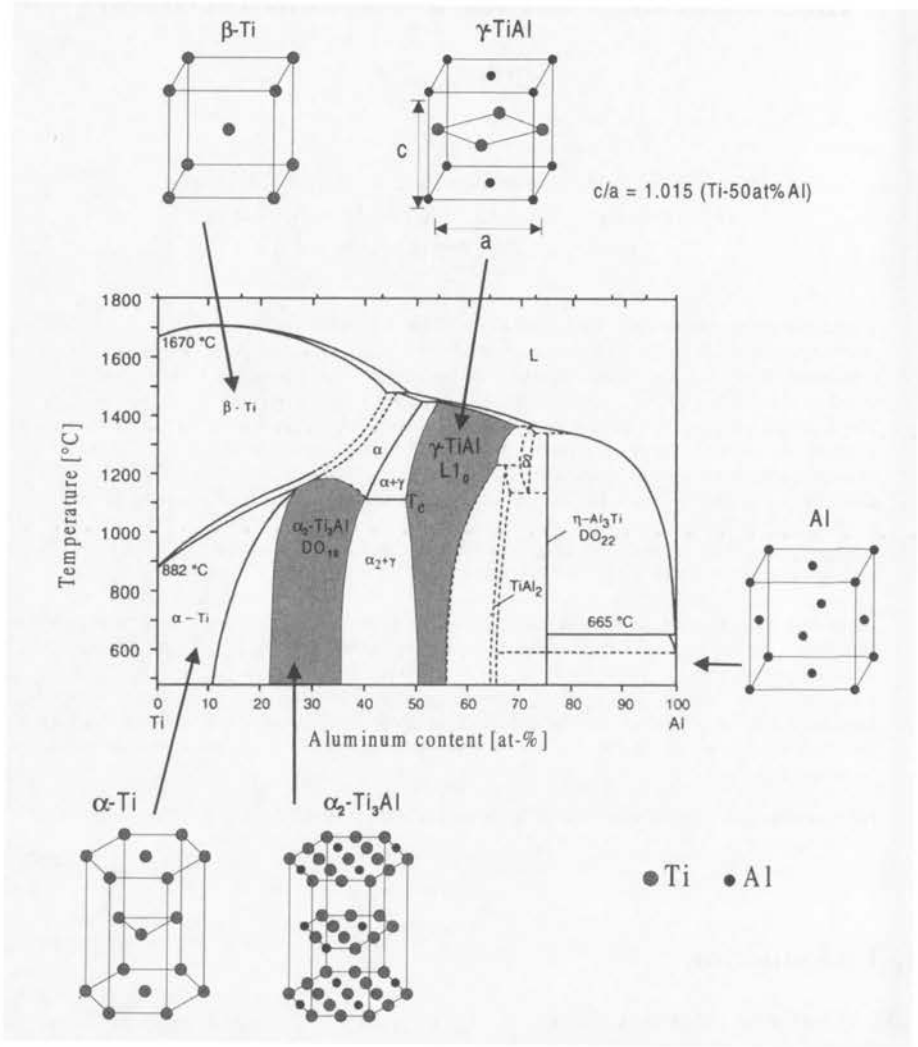

FIGURE 1. Ti-Al binary phase diagramm and sketches of the occuring crystal structure depending on the Aluminium content.

The knowledge of intermetallics is by no means new in metal physics. However, their application as a (structural) material is rather new. To the author's view shape memory alloys (SMAs) are the best known representatives of intermetallics (e.g. Nitinol), which have gained a growing relevance for technical applications, however, not for their strength but for the shape memory effect having its origin

in a martensitic transformation. We do not intend in this manuscript to deal with SMAs. We move back to TiAl intermetallics which are a realistic candidate for a new, high strength material due to its high temperature behaviour and its low weight.

It should be mentioned that intermetallics play a role in several kinds of metals in the form of precipitations. Usually they are not appreciated due to their brittleness. Sometimes, they are used as substitutes of carbides, e.g. in tool steel, due to their strong brittleness and their better wear resistant behaviour compared to "classical" hard particles like carbides.

Typical applications of TiAl intermetallics are found in those fields of design demands, where low weight and high temperature resistance play a major role. Let us look at three "typical" applications:

- Temperature protection systems (TPSs) being operative in the temperature range up to ca. 800°C. Typical applications can be seen in the "new" space shuttle of the NASA, as in the first step in one of the prototypes with the name X-33 (the "1/3" model of the future shuttle).
- Turbine blades, specifically in the low pressure part of gas turbines. The fact that these blades are 50% lighter compared to blades made from the classical superalloys changes the dynamic regime of such a blade and its surroundings. Note the increase of the velocity of sound by a factor $\sqrt{2}$ compared to superalloys!
- Valves in combustion engines, e.g. for cars. Typical valves of "conventional" steel have a weight of appx. 50 gr, those of TiAl of appx. 30 gr. It should be noted that TiAl valves have already proven to work successful in cars having run more than 100 000 km. The main advantage is the low weight with respect to a better dynamic control e.g. by electronic devices. Compared to ceramics TiAl intermetallics are superior at higher temperatures due to the increasing ductility.

1.2. Properties of TiAl intermetallics

The last ten years have witnessed a rapid growth in the study and the understanding of intermetallic compounds. A permanently increasing part of this progress has been directly achieved by the introduction of computational modelling to contribute to the urgent investigations of experimentalists and the incessant call of industry for new and better materials for advance engineering applications.

In particular, intermetallic γ-TiAl-based alloys have been a good example for the fruitful interaction between fundamental and applied research and industrial development which, both together, lead to a new class of advanced engineering materials. It is due to their attractive properties that γ-TiAl-based alloys are considered for high-temperature applications in aerospace and automotive industries (Kim, 1994; Kim, 1989; Kim and Dimiduk, 1991; Clemens, 1995; Clemens et al., 1999; Bartalotta and Krause, 1999; LeHolm et al., 1999; Tetsui, 1999, Blum et al., 1999; Clemens and Kestler, 2000; Knippscheer and Frommeyer, 1999). These properties include low density ($\sim 3.8\,\mathrm{g/cm^3}$), high specific yield strength (yield strength/density), high specific stiffness (modulus of elasticity/density), good oxidation resistance, resis-

tance against "titanium fire", and good creep properties up to high temperatures. Above all, the high specific stiffness which is retained at elevated temperatures is most advantageous for the design of light-weight structural parts. In spite of these promising high-temperature properties, the low ductility and fracture toughness at room temperature have limited their commercial application so far.

Intense research over the last years has led to a better understanding of the fundamental influence of alloy composition and microstructure on mechanical properties and processing behavior. Industry appears to be on the threshold of significant use of this new class of materials. In particular, all major aircraft and automotive engine manufacturers are advancing the qualification and introduction of γ-TiAl components. γ-TiAl-based alloys can be processed using conventional metallurgical methods – a factor, which is necessary for these specific materials to be economically competitive with other state-of-the-art materials. The processing of γ-TiAl alloys via ingot- and powder metallurgical routes on industrial scale has been successfully demonstrated. However, for widespread application of γ-TiAl alloys it must be guaranteed, that semi-finished products as well as components with specified mechanical properties can be manufactured in large quantities at reasonable cost. Furthermore, for structural applications, appropriate joining and repairing methods must be available which guarantee the processing of reliable joints exhibiting good mechanical properties especially at temperatures below the brittle-to-ductile transition temperature.

Engineering γ-TiAl-based alloys should exhibit a more improved balance between room temperature ductility, fracture toughness, high-temperature strength, creep and oxidation resistance. Presently, next-generation γ-TiAl-based alloys are under development aiming to provide these improved properties (Clemens and Kestler, 2000).

Two-phase γ-TiAl-based alloys of engineering interest consist of γ-TiAl (ordered face-centered tetragonal $L1_0$ structure) and α_2-Ti_3Al (ordered hexagonal DO_{19}-structure). The γ-TiAl phase exhibits a tetragonal phase centered (fct) crystal structure with a low c/a axial ratio ($c/a \approx 1.02$) and is composed of alternating planes of Ti and Al atoms in the [001] direction. In thermodynamic equilibrium the γ/α_2-volume fraction is controlled by the Al-content and additional alloying elements and typically is in the range of 0.05 to 0.2 (Kim, 1989; Kim, 1994). However, thermomechanical processing and heat treatments have a strong influence on the actual γ/α_2-volume fraction in γ-TiAl-based alloys (Clemens and Kestler, 2000). Although the single α_2-Ti_3Al phase is more brittle than the γ-TiAl phase it has a significant effect on the mechanical properties, deformation behavior and ductility of γ-TiAl-based two phase alloys. In contrast to single phase γ-TiAl, mechanical twinning as an additional deformation mechanism is activated (Kim, 1989; Hall and Huang, 1991; Appel and Wagner 1998).

The composition (in at.%) of conventional engineering γ-TiAl-based alloys can be summarized as follows:

$$Ti_{45\text{-}52} - Al_{45\text{-}48} - X_{1\text{-}3} - Y_{2\text{-}5} - Z_{<1},$$

where

$$X = \text{Cr, Mn, V,} \qquad Y = \text{Nb, Ta, W, Mo,} \qquad Z = \text{Si, B, C.}$$

The alloying elements marked with X, Y, and Z all affect more or less the position of the phase boundaries in the Ti-Al binary phase diagram (Kim, 1989; Kim and Dimiduk, 1991; Kattner et al., 1992; Hall and Huang, 1991). While Cr, Mn and V lower the stacking fault energy and thus increase the ductility of the alloys at room temperature by increasing the propensity for mechanical twinning, the other alloying elements improve the high temperature properties (e.g. resistance to oxidation, creep strength). Boron is typically used as a grain refining agent. Engineering γ-TiAl-based alloys contain at least one ductilization element and one refractory element which improves oxidation and creep resistance. However, the creep resistance of these alloys seems to limit the maximum application temperature to 700°C, especially if long-term service is considered. This is probably a direct consequence of thermally activated dislocation processes which make the mechanical behavior of γ-TiAl alloys strongly rate-dependent. Additional limitations might arise from microstructural instabilities (Chatterjee, 2000), which are also expected to degrade the creep properties, and from an insufficient oxidation resistance at temperatures exceeding 700°C (Brady et al., 1996). In order to increase the high-temperature capabilities of γ-TiAl-based alloys, current alloy development programs are focused on high Nb containing alloys as well as C containing alloys (Kim, 1994; Appel et al., 1999a; Appel et al., 1999b).

Appropriate thermomechanical treatments and/or heat treatments can be applied to achieve various microstructures. A microstructural classification system has been proposed by Kim, 1994, which defines four types of microstructure: near-gamma, duplex, nearly lamellar and fully lamellar. The processing routes on industrial scale established for γ-TiAl-based alloys are reported in detail by Clemens and Kestler, 2000. Generally, the influence of microstructure on mechanical properties of γ-TiAl-based alloys can be summarized as follows: coarse-grained fully lamellar microstructures exhibit relatively good fracture toughness and excellent creep resistance, but poor tensile ductility and strength especially at room temperature. Relatively fine-grained equiaxed primary annealed, near-gamma, duplex microstructures with only small amounts of lamellar colonies show low fracture toughness and creep resistance but moderate tensile ductility and strength at room temperature and elevated temperatures. This inverse correlation between tensile properties and resistance to fracture needs a careful selection of the microstructure remaining unchanged during service.

1.3. Micromechanical research goals

The present manuscript can be divided into two parts:

1. The first part starting with a room temperature investigations on polycrystalline near-γ TiAl based alloys. An experimental study is combined with micromechanical modelling in order to investigate the deformation behavior at room temperature of a two-phase γ-TiAl based alloy with near-γ microstructure. Uniaxial compression tests are carried out at room temperature applying different strain rates. Accompanying acoustic emission during deformation was monitored and revealed the formation of mechanical twins as an important

mode of plastic deformation. The deformation behavior of the γ-TiAl alloy is simulated, and the contribution of deformation twinning to the total plastic deformation is analyzed. Results of the simulations and experimental data are compared and discussed.

2. The second part of the work comprises a numerical simulation of the creep behavior of a lamellar γ-TiAl alloy based on intense accompanying experimental research. Based on the assumption that interface spacing of the lamellar colonies has a major influence on the creep behavior differently spaced DFL microstructures were adjusted in order to investigate their influence on creep. Short term creep tests were carried out in air at 700°C and 800°C under a load stress of 175 MPa constant in time. The interface spacing was varied in the range of 1.2 μm to 0.14 μm by altering the cooling rates from 1 K/min to 200 K/min. A first approach in modelling the steady state creep deformation of the fully lamellar material in question is presented. A power law description for diffusion controlled dislocation creep is proposed, and a structure factor is introduced which depends on the lamellar orientation with respect to the loading axis as well as on the mean lamellar interface spacing.

1.4. An introductory remark

The author considers the experimental basis provided by Prof. H. Clemens and his cooperators of inestimable value being a necessary precondition for both the conception of micromechanical models and their validation. Prof. H. Clemens, now with GKSS Research Center, Geesthacht, D, formerly with the Institute of Physical Metallurgy, University of Stuttgart, D, as well as Plansee AG, Reutte, A, has accompanied our modelling activities for several years and provided us with the most relevant experimental data. He gave us detailed information on the mechanisms behind a deformation process. In addition he provided us also with information on presumptive technological applications and the technological relevance of our common modelling findings.

With respect to modelling the author refers to Mrs. S.M. Schlögl as the first doctoral researcher and Mr. W.T. Marketz as the second doctoral researcher. Their works have formed the basis of our micromechanical models and can be found in several publications. The author would like to cite here the printed versions of their theses:

- S.M. SCHLÖGL, *Micromechanical Modelling of the Deformation Behaviour of Gamma Titanium Aluminides*, Fortschritt-Berichte VDI, Reihe 18, Nr. 220, 1997.
- W.T. MARKETZ, *Micromechanical Modeling of the Deformation Behavior of Polycrystalline γ-TiAl Based Alloys*, Fortschritt-Berichte VDI, Reihe 5, Nr. 624, 2001.

Finally it should be mentioned that our group will start their next project together with Prof. H. Clemens, namely the modelling of forming (forging) of as-cast lamellar microstructures, their "internal" buckling and the role of recrystallization.

2. Room temperature deformation behavior of polycrystalline γ-TiAl

2.1. Deformation mechanisms and their continuum mechanical description

The deformation modes of γ-TiAl based alloys strongly depend on their microstructure, their alloy composition and the temperature. On the basis of pioneering studies (Shechtman et al.,1974; Sastry and Lipsitt, 1977) it is now well established (Appel and Wagner, 1998; Yamaguchi and Umakoshi, 1990; Inui et al., 1992) that that deformation of γ-TiAl under most conditions occur on $\{111\}$ planes by glide of ordinary dislocations with the Burgers vector $b = 1/2\langle 110]$ and superdislocations with the Burgers vector $b = \langle 101]$ and $b = 1/2\langle 11\bar{2}]$, respectively. In addition mechanical twinning along $1/6\langle 11\bar{2}]\{111\}$ occurs that does not alter the ordered $L1_0$ structure of γ-TiAl. The mixed notation $\langle uvw]$ indicates a set of equivalent crystallographic directions generated by permutations of $\pm u$ and $\pm v$, while the index w is held fixed. Figure 2 shows the potential slip and twinning systems of the $L1_0$ structure, while in Table 1 all the possible deformation mechanisms are listed.

One can see from Fig. 2 that along the $\langle 110]$-directions there is only one sort of atoms (either Ti or Al). This type of dislocations is called ordinary dislocations. By contrast Ti-atoms and Al-atoms interchange in $\langle 011]$-directions and, therefore, the so called superdislocations must operate in $\langle 011]$-directions which are dissociated into two $1/2\langle 101]$-dislocations separated by an antiphase boundary (APB). Additionally, the $L1_0$ structure can be twinned by the $\{111\}\langle 11\bar{2}]$ variants of the normal fcc twinning mode. As can be seen in Fig. 2, the Burgers vector $b_3 = 1/6[11\bar{2}]$ preserves the order of γ-TiAl and this twinning mode is, therefore, called true twinning.

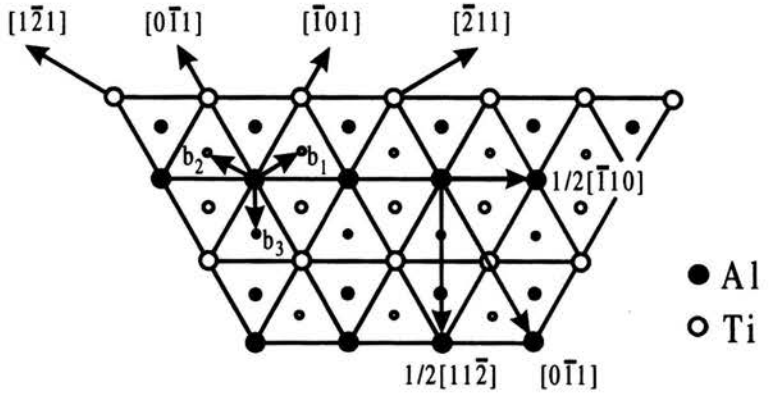

FIGURE 2. Potential slip and twinning systems of the $L1_0$ structure, schematic drawing of a three-layer sequence of atom stacking on the $\{111\}$ plane shown by small, medium and large circles. $b_1 = 1/6[\bar{2}11]$, $b_2 = 1/6[1\bar{2}1]$ and $b_3 = 1/6[11\bar{2}]$ are the Burgers vectors of partial dislocations. b_3 is perpendicular to the Burgers vector $b = 1/6[\bar{1}10]$ for ordinary dislocations and represents the Shockley partial dislocation for true twinning, whereas b_1 and b_2 represent pseudo-twinning (after Appel and Wagner, 1998).

TABLE 1. Slip systems of ordinary dislocations and superdislocations and true twinning in γ-TiAl.

Slip/Twin plane	Slip direction ordinary dislocation	Slip direction super dislocation	Twinning direction
(111)	$[\bar{1}10]$	$[0\bar{1}1]$ $[10\bar{1}]$	$[11\bar{2}]$
$(\bar{1}11)$	[110]	[101] $[0\bar{1}1]$	$[\bar{1}1\bar{2}]$
$(1\bar{1}1)$	[110]	[011] $[10\bar{1}]$	$[1\bar{1}\bar{2}]$
$(11\bar{1})$	$[\bar{1}10]$	[011] [101]	[112]

Partial dislocations by Burgers vectors $b_1 = 1/6[\bar{2}11]$ and $b_2 = 1/6[1\bar{2}1]$, respectively, change the order of γ-TiAl and theses modes are called pseudo twinning. The relative contributions of the individual mechanisms to the deformation mainly depend on the aluminium concentration, the content of ternary elements and the deformation temperature (Appel and Wagner, 1998).

In the α_2-Ti_3Al phase the possible slip modes are: $\{10\bar{1}0\}\langle\bar{1}\bar{2}10\rangle$ prism slip, $(0001)\langle\bar{1}\bar{2}10\rangle$ basal slip and pyramidal $\{11\bar{2}1\}\langle11\bar{2}\bar{6}\rangle$-slip with very different values of critical shear stresses (Umakoshi et al., 1993).

2.1.1. Crystallographic slip. The constitutive theory used in the room-temperature (RT) analysis is a rate dependent formulation rigorously accommodating finite deformation effects. The plastic deformation is assumed due solely to crystallographic slip and deformation twinning, whereas deformation by diffusion or grain boundary sliding is not considered here. The presented kinematical theory of the mechanics of crystals is based on the studies of Hill, 1966, Hill and Rice,1972, Asaro and Rice, 1977 and the extension of this basic formulation into a rate dependent description by Asaro, 1983, Peirce et al., 1983 and Asaro and Needleman, 1985. For a detailed description of the continuum theory of plasticity we also refer to Khan and Huang, 1995.

The applied crystal plasticity concept is a physically motivated one with plastic deformation being the result of continuous shearing or slip along various, well-defined lattice planes. A slip system α is defined by the pair of orthogonal unit vectors $\mathbf{s}^{(\alpha)}$ and $\mathbf{m}^{(\alpha)}$. The unit vector in slip direction of slip system α is denoted by $\mathbf{s}^{(\alpha)}$, and $\mathbf{m}^{(\alpha)}$ denotes the unit vector normal to the slip direction.

The specific relation applied in the calculation is a power law description previously employed by Peirce et al., 1983, Asaro et al., 1985 or Kad et al.,1995,

$$\dot{\gamma}^{(\alpha)} = \dot{\gamma}_0^{(\alpha)} \operatorname{sign} \tau^{(\alpha)} \left| \frac{\tau^{(\alpha)}}{g^{(\alpha)}} \right|^{\frac{1}{m}}, \tag{2.1}$$

where the shear rate $\dot{\gamma}^{(\alpha)}$ on the slip system α is determined by the resolved shear stress $\tau^{(\alpha)}$, $g^{(\alpha)}$ is the current strength of the system, $\dot{\gamma}_0^{(\alpha)}$ is the reference shear rate while m represents the strain rate sensitivity of the material. In the limit $1/m \to \infty$ Eq. (2.1) approximates a strain rate independent material behavior.

The resolved shear stress $\tau^{(\alpha)}$ on the slip system α is given by

$$\tau^{(\alpha)} = \mathbf{P} : \sigma, \tag{2.2}$$

with the Schmid tensor defined as

$$\mathbf{P}^{(\alpha)} = \frac{1}{2}\left(\mathbf{s}^{*(\alpha)} \otimes \mathbf{m}^{*(\alpha)} + \mathbf{m}^{*(\alpha)} \otimes \mathbf{s}^{*(\alpha)}\right). \tag{2.3}$$

The initial conditions for $g^{(\alpha)}$ at $\gamma = 0$ ($\gamma = \sum_\alpha \int |\dot{\gamma}^{(\alpha)}|\, dt$) has to be specified, and this material parameter is denoted by $\tau_0^{(\alpha)}$ and represents the initial slip system hardness of slip system α. The strain hardening is characterized by the evolution of $g^{(\alpha)}$ by the incremental relation

$$\dot{g}^{(\alpha)} = \sum_\beta h_{\alpha\beta}\, \dot{\gamma}^{(\beta)}, \tag{2.4}$$

where $h_{\alpha\alpha}$ is the self hardening modulus and $h_{\alpha\beta}$ is the latent hardening modulus. For $h_{\alpha\alpha}$ we use the following form proposed by Peirce et al., 1982,

$$h_{\alpha\alpha} = h(\gamma) = h_0 \sec h^2 \frac{h_0\, \gamma}{\lambda_s^{(\alpha)} - \tau_0^{(\alpha)}}, \tag{2.5}$$

where h_0 represents an initial hardening rate and $\tau_s^{(\alpha)}$ denotes a saturation strength. The latent hardening modulus is given by

$$h_{\alpha\beta} = q\, h(\gamma), \tag{2.6}$$

with q as a constant lying in the range of $1 \leqslant q \leqslant 1.4$.

2.1.2. Deformation twinning. In addition mechanical twinning along $1/6\,\langle 11\bar{2}]\,\{111\}$ occurs that does not alter the $L1_0$-structure. There is growing evidence that the activation of ordinary dislocations and superdislocations requires significantly different shear stresses so that the different dislocation glide systems often cannot simultaneously operate. In this respect, the activation of mechanical twinning may compensate the lack of independent glide systems which can operate at comparable stresses and, thus, support the plasticity of polycrystalline materials (Appel, 1999c). However, these deformation mechanisms, which are restricted to {111} planes can cause locally a very high anisotropy which is, additionally, increased by the unidirectionality of twinning. While slip can operate in the positive as well as in the negative slip direction, the twinning shear is always directional in the sense that shear in one direction is not equivalent to shear in the opposite direction. In our case of tetragonal face centered γ-TiAl crystals twinning occurs by shear on the (111) plane in the $\langle 11\bar{2}]$ direction but not by shear in the $\langle \bar{1}\bar{1}2]$ direction (Hosford, 1993).

However, an already formed twin can be annihilated by a shear in the opposite direction (i.e. detwinning).

Twinning is a deformation mechanism involving shear displacements on specific crystallographic planes, i.e. twinning planes K_1, along specific crystallographic directions, i.e. twinning directions η_1 (see Fig. 3). The magnitude of the shear displacement on a slip plane is variable, but it always corresponds to an integer number of interatomic distances. As to twinning, the shear displacement is a fraction of the interatomic distance.

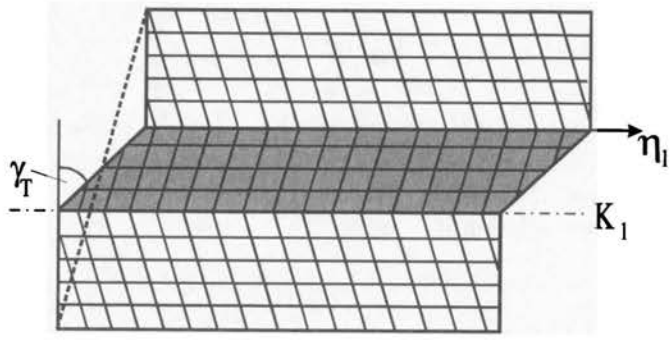

FIGURE 3. Production of a twin by homogeneous shear of the lattice on the plane K_1 in the direction η_1. γ_T denotes the twinning shear and the dashed line indicates the average shear of the material volume (after Schlögl, 1997).

Compared to slip, twinning necessitates shear on every successive plane. To become a twin, one part of the crystal must undergo a certain shear, which is determined by the lattice. This so called twinning shear γ_T has the value $1/\sqrt{2}$ in the case of γ-TiAl. In our finite element calculations stresses and strains are computed as averaged values over a material volume pertaining to the integration point under consideration. Such a material volume is "large" compared to the existing mechanical twins. Schlögl and Fischer, 1997, proposed the following "averaging" description:

Due to the formation of a twin β with a volume fraction $f^{(\beta)}$ the average shear $\gamma^{(\beta)}$ is equal to $\gamma_T\, f^{(\beta)}$. Consequently, the shear rate $\dot{\gamma}^{(\beta)}$ is connected with the rate of $f^{(\beta)}$ in the following way:

$$\dot{\gamma}^{(\beta)} = \gamma_T \dot{f}^{(\beta)} \quad \text{with} \quad \dot{f}^{(\beta)} = \dot{f}_0^{(\beta)} \left(\frac{\tau^{(\beta)}}{\tau_0^{(\beta)}} \right)^{\frac{1}{m}}, \tag{2.7}$$

where $\dot{f}_0^{(\beta)}$ is a reference twinning rate.

To account for $\dot{f}^{(\beta)}$ (Christian and Mahajan, 1995) it has been postulated that twinning operates above a threshold $\tau_0^{(\beta)}$ analogous to Schmid's law for crystallographic slip. This means that the shear stress $\tau^{(\beta)}$ across the twinning plane, resolved in the twinning direction, is the driving force for the nucleation and growth of the twin β. If $\tau^{(\beta)}$ reaches the value of the critical shear stress for twinning, $\tau_0^{(\beta)}$, twin nucleation is assumed to have occurred in the volume pertaining to the con-

sidered integration point. At an integration point, the unidirectionality mentioned above is considered as follows:

$$\begin{aligned} &\text{if } \tau^{(\beta)} \leqslant 0, && \text{then} && \dot{f}^{(\beta)} = 0, \\ &\text{if } \tau^{(\beta)} > \tau_0^{(\beta)} > 0, && \text{then} && \dot{f}^{(\beta)} \neq 0. \end{aligned} \tag{2.8}$$

2.1.3. Slip and twinning. Both mechanisms, slip and twinning, can operate in the considered volume elements. It is assumed that slip does not occur in the twinned zones. Therefore, the average inelastic strain rate of a volume element ν is

$$\dot{\varepsilon}_{in}^{\nu} = (1 - f^{\nu}) \sum_{\alpha=1}^{12} P^{(\alpha)} \dot{\gamma}^{(\alpha)} + \sum_{\beta=1}^{4} P^{(\beta)} \gamma_T \dot{f}^{(\beta)}. \tag{2.9}$$

The α and β indices stand for slip and twinning systems, respectively, and f^{ν} for the total twinned volume fraction in the considered volume element,

$$f^{\nu} = \sum_{\beta=1}^{4} f^{(\beta)}. \tag{2.10}$$

In addition to the presented formulation there has been a considerable advance in the description of deformation twinning, e.g. by Staroselsky and Anand, 1998, using a random selection procedure scheme to determine the active systems and the shear increments on active twin systems. Kalidindi, 1998, reports an alternative incorporation of deformation twinning in crystal plasticity models. Srinivasa et al., 1998, published a phenomenological model of twinning based on dual reference structures. The onset of twinning is determined purely by energy considerations. Additionally, we want to refer to a paper by Lee and Yoo, 1990, dealing with the elastic strain energy of deformation twinning in tetragonal crystals.

2.2. Acoustic emission (AE) measurements

The purpose of this combined experimental and computational work is an investigation of the deformation mechanisms of polycrystalline near-γ material using both computational finite element (FEM) simulations and acoustic emission (AE) measurements. A three-dimensional micromechanical model, initially developed to describe lamellar γ-TiAl single crystals [35], has been adjusted to simulate the deformation behavior of polycrystalline near-γ material. The aim of the studies is to point out the role of deformation twinning during the deformation process. The contribution of twinning to the total plastic deformation is computed investigating compression tests at room temperature applying different strain rates. It is intended to clarify the onset of twinning combining results of our simulation with experimental data obtained from AE measurements.

AE-analysis is a well-suited method which allows a rapid detection of micromechanical events such as avalanche dislocation movement, mechanical twinning and microcracking (Heiple and Carpenter, 1987). The aim of the AE-investigations in

this work is to correlate the AE-signal with the corresponding microstructural deformation process by compressive testing of TiAl alloy described above. Cylindrically shaped specimens (ϕ 10 mm, length 20.0 mm) with a flat face parallel to the specimen length were cut from bulk material and polished. Specimens were axially compressed between flat hard metal (WC-Co) punches at a constant strain rate using a screw-driven testing machine.

In order to investigate the effect of strain rate on deformation behavior three different strain rates were applied: $2 \cdot 10^{-3}\,s^{-1}$, $2 \cdot 10^{-4}\,s^{-1}$ and $2 \cdot 10^{-5}\,s^{-1}$. Thin Teflon®-foils were placed between the specimen and the punches to avoid AE from friction. Strain was measured by an extensometer that was directly clamped to the specimen. Figure 4 shows the experimental set-up of the AE monitoring measurements. Continuous AE monitoring was accomplished with a root mean square (RMS) voltmeter (Model 3400A, Hewlett Packard). More details on the experimental procedure are reported by Bidlingmaier et al., 1999. In order to avoid artifacts several experiments on dummy specimens of other materials were performed. These experiments proved that frictional effects at the specimen/punch interfaces and other possible contributions from the loading system play no significant role.

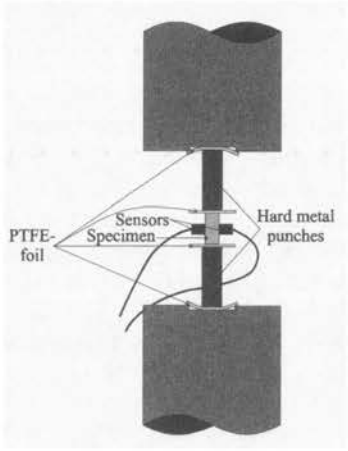

FIGURE 4. Sketch of the experimental set-up for acoustic emission (AE) measurements (Kauffmann, 1999).

2.3. Micromechanical modelling

Based on the micromechanical model developed by Schlögl and Fischer, 1997, to simulate the deformation behavior of polysynthetically twinned (PST) single crystals of lamellar TiAl, the model has been extended to describe polycrystalline TiAl. The intention has been to simulate displacement controlled uniaxial tensile- and compression tests.

For the simulation a representative volume element (RVE) in cubic shape has been chosen. Periodic boundary conditions are enforced on the surface of the RVE. To account for the grain shape one has to ensure that the cubic RVE can be filled by these grains without voids.

The first developed RVE (unit cell 1, Fig. 5) consists of one layer of 24 hexagonal γ-TiAl grains with defined (texture) or random orientation. The finite element mesh consists of 727 20-node quadratic brick elements and 146 15-node quadratic triangular prism elements (Schlögl, 1997).

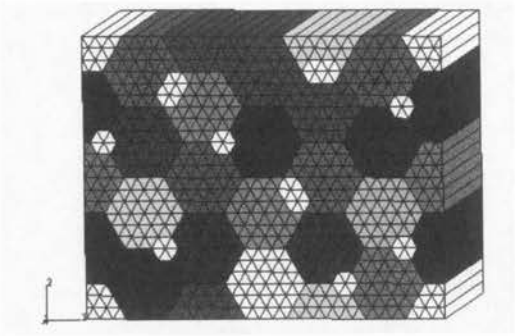

FIGURE 5. RVE for the near-γ microstructure with 24 hexagonal γ-TiAl grains (dark) and 5 vol% α_2-Ti_3Al (white) located at triple junctions and grain boundaries.

It is obvious that in this pseudo three-dimensional unit cell one direction is favored above the other two. As a further step to a fully three-dimensional model brick shaped grains have been chosen. This time the cubic RVE (unit cell 2) consists of 64 γ-grains arranged irregularly. Furthermore, the α_2-phase is located randomly at grain boundaries and triple junctions. One cubic γ-grain consists of 50 to 70 8-node linear brick elements. The RVE is shown in Fig. 6.

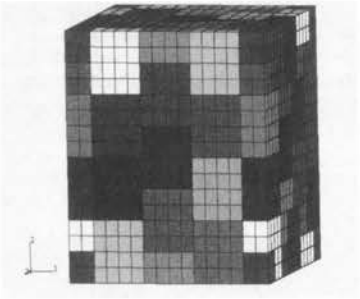

FIGURE 6. RVE for the near-γ microstructure with 64 γ-TiAl grains indicated by the different shades of grey. The α_2-phase is not indicated in the figure but located at the grain boundaries.

At least a cubic RVE filled with rhombic dodecahedral grains has been developed. The finite element mesh consists of 10-node quadratic tetrahedral elements. One γ-grain consists of 192 10-node quadratic tetrahedral elements and exhibits good symmetry properties. This feature and the more realistic shape of the grains are supposed to avoid artificial local "stiffness" in the FEM-calculation. As can be seen in Fig. 8 the α_2-phase is located randomly at triple junctions and grain boundaries.

As already mentioned above, periodic boundary conditions are used to ensure periodicity. This means that the difference between the displacement vectors of two corresponding points situated at opposite unit cell boundaries is a constant displacement vector for pairs of corresponding points. Furthermore, periodic boundary conditions are necessary that a cube can be filled with rhombic dodecaeders. If one looks at Fig. 7, the constraints can be expressed by the following relations:

$$\begin{aligned} \mathbf{u}(x,y,h) - \mathbf{u}(x,y,0) &= \mathbf{k}_1, \\ \mathbf{u}(l,y,z) - \mathbf{u}(0,y,z) &= \mathbf{k}_2, \\ \mathbf{u}(x,b,z) - \mathbf{u}(x,0,z) &= \mathbf{k}_3, \end{aligned} \tag{2.11}$$

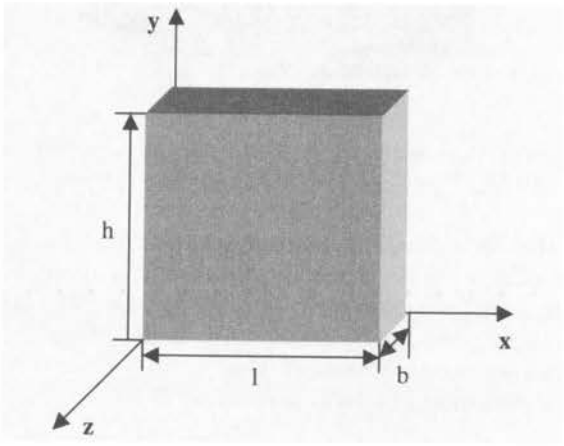

FIGURE 7. RVE and coordinate system in order to explain the constraints to ensure periodic boundary condition according to Eq. (2.11). In case of a cubic RVE filled with rhombic dodecahedral grains (see Fig. 6) $l = b = h$.

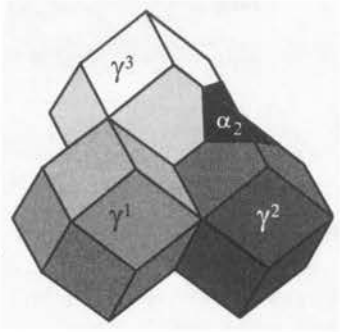

FIGURE 8. Detail of the three dimensional RVE showing three γ-TiAl grains (γ^1, γ^2, γ^3) and the α_2-phase located at grain boundaries.

where $\mathbf{u}(x, y, z)$ is the displacement vector of a point with the coordinates (x, y, z), and $\mathbf{k}_1$, $\mathbf{k}_2$, $\mathbf{k}_3$ are constant displacement vectors which may be prescribed or follow global equilibrium conditions of the RVE.

The elastic constants of the γ-phase used in the model are listed in Table 2. They originate from first principle calculations (Yoo et al., 1991). Since the tetragonality of the γ-TiAl phase is small with the c/a ratio of 1.015, this phase is treated like a fcc-crystal. An amount of 5 vol% of the α_2-phase and the B2-phase is located randomly at triple junctions and grain boundaries. In a first attempt the B2-phase is treated totally elastic with equivalent properties as for α_2-Ti_3Al. The elastic constants of the α_2-phase are listed in Table 3.

TABLE 2. Calculated elastic constants of γ-TiAl.

E_{1111}	E_{1122}	E_{2222}	E_{1133}	E_{3333}	E_{1212}	E_{1313}	E_{2323}
190 GPa	105 GPa	190 GPa	90 GPa	185 GPa	50 GPa	120 GPa	120 GPa

TABLE 3. Calculated elastic constants of α_2-Ti_3Al.

E_{1111}	E_{1122}	E_{2222}	E_{1133}	E_{3333}	E_{1212}	E_{1313}	E_{2323}
221 GPa	71 GPa	221 GPa	85 GPa	238 GPa	75 GPa	69 GPa	69 GPa

According to the theoretical comments in Sec. 2.1, the micromechanical model for γ-TiAl based two phase alloy must take into account different deformation modes, which depend strongly on their microstructure, their alloy composition and the temperature. The following glide and twinning systems will be considered in the model.

Glide of ordinary dislocations (Burger's vector $b = 1/2\langle 110]$) and super dislocations (Burger's vector $b = \langle 101]$ and $b = 1/2\langle 11\bar{2}]$), respectively, on $\{111\}$-planes of the γ-TiAl phase. In addition, mechanical twinning along $1/6\langle 11\bar{2}]\{111\}$ occurs. In the α_2-Ti_3Al phase the considered slip modes are $\{10\bar{1}0\}\langle\bar{1}\bar{2}10\rangle$ prism slip, $(0001)\langle\bar{1}\bar{2}10\rangle$ basal slip and pyramidal $\{11\bar{2}1\}\langle 11\bar{2}\bar{6}\rangle$-slip.

The critical resolved shear stress (CRSS) $\tau_0^{(\alpha)}$ for ordinary dislocation glide on slip system α, i.e. the slip system hardness $g^{(\alpha)}$ at a shear $\gamma = 0$, is accounted for by the Hall-Petch effect, and therefore, $\tau_0^{(\alpha)}$ is taken to depend on the grain size as

$$\tau_0^{(\alpha)} = \tau_R + \frac{k_y}{\sqrt{d_a}}, \tag{2.12}$$

where d_a denotes the average diameter of the globular near-γ grains and corresponds to the mean free path length of the dislocations in the material. With reference to experimental investigations (Umakoshi et al., 1993) the following expression is proposed:

$$\tau_0^{(\alpha)} = 70 + 0.27\, d_a^{-\frac{1}{2}}. \tag{2.13}$$

A user-defined material subroutine (Schlögl, 1997; Huang, 1991) was used to implement the constitutive behavior of the γ-TiAl phase and the α_2-Ti_3Al phase

within the framework of crystal plasticity described in Sec. 2.1. The field equations are solved with the finite element package ABAQUS.

2.3.1. Calibration of the model. In order to calibrate the model, i.e. to determine the constants in the presented theoretical concept (Sec. 2.1), the deformation behavior of a rolled Ti-48Al-2Cr sheet material has been simulated. The sheet under consideration has been annealed at 1000°C for 2 hours and then the near-γ heat-treatment was conducted (1200°C/2hr + 1000°C/3hr). As a consequence the material exhibits a weak texture and a grain size of about $d_a = 20\,\mu$m. The tests and the simulation has been carried out in tension.

According to Eqs. (2.1), (2.7) and (2.13) the following parameters were taken:

- Since twinning is described as a unidirectional slip mechanism, we chose the same CRSS value for twinning ($\tau_0^\alpha = \tau_0^\beta = 130\,$MPa).
- The contribution of super-dislocations to the deformation behavior of two-phase γ-TiAl based alloys is smaller (Appel and Wagner, 1998), and therefore, a higher CRSS $\tau_0^{\text{super}} = 200\,$MPa is chosen.
- In this first attempt the α_2-phase is estimated to exhibit only isotropic and elastic deformation with a Young's modulus of E=148 GPa and a Poisson's ratio of ν=0.29 (Schafrik, 1977). This assumption does not influence the deformation behavior of the whole specimen since the α_2-phase is harder than the γ-phase and the volume fraction is small.

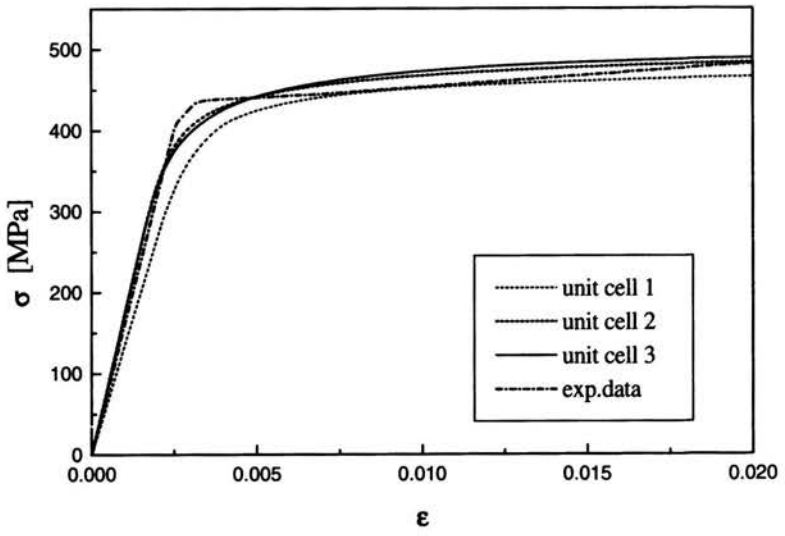

FIGURE 9. Uniaxial tensile behavior of Ti-48at%Al-2at%Cr sheet material. Comparison of the experimental data (strain rate $\dot{\varepsilon} = 10^{-4}\,\text{s}^{-1}$) with the simulation considering three different models of grain-shapes:
unit cell 1: one layer of hexagonal γ-TiAl grains,
unit cell 2: 64 cubic grains, arranged irregularly,
unit cell 3: 32 rhombic dodecahedral grains.

- $\dot{\gamma}_0^{(\alpha)}$ is constant for all slip systems and is selected as $0.001\,s^{-1}$. In accordance with the experimentally observed low strain rate sensitivity (Mendiratta et al., 1993) a value 0.01 for m is chosen. Furthermore, hardening is assumed to be the same for all slip systems. As to twinning, the reference twinning rate (see Eq. (2.7)) is $\dot{f}_0^{(\beta)} = 0.0014\,s^{-1}$. There has been attributed no hardening to twinning. However, if a twin is formed, the twin area is restricted for any other deformation mechanism. This accounts for the reduction in slip path length since a twin acts as a new barrier (e.g. interface) for slip.

In Fig. 9 the results of the simulation of the global stress strain behavior of the weak textured Ti-48Al-2Cr sheet material is depicted. The simulation has been carried out for a tensile test in the rolling direction, and the results of the RVEs consisting of the three different grain shapes are compared to experimental data. As can be seen, the model with the cubic grain shape cannot reproduce the stress strain behavior of the material very well. The disadvantage of the model with the hexagonal brick shaped grains is the restriction to only two dimensions. As a consequence it turns out that the RVE exhibiting rhombic dodecahedral grains can reproduce the deformation behavior of the TiAl alloy best. A closer look to the local stress behavior reveals that this RVE avoids artificial local "stiffness" in the FEM-calculation (Marketz et al., 1999).

2.3.2. Investigation of a Ti-46.5at%Al-4at%(Cr,Nb,Ta, B) near-γ alloy. The Ti-46.5at.%Al-4at.%(Cr, Nb,Ta, B) material was produced via a powder-metallurgical route. The gas atomized γ-TiAl alloy powder was hot-isostatically pressed in two steps: 1.5 hours at 1270°C and a pressure of 200 MPa followed immediately by 2 hours at 1000°C and 150 MPa. By this HIP-treatment a homogeneous fine grained globular near-γ microstructure (Kauffmann et al., 2000, Kauffmann, 1999) was obtained as shown in Fig. 10. The present microstructure consists of γ-TiAl phase ($L1_0$-structure) and a volume fraction of less than 10% of the α_2-Ti_3Al phase ($D0_{19}$-structure) and of a Cr enriched B2-phase (CsCl-structure) located at grain boundaries and triple junctions of the equiaxed γ-grains. Additionally, (Ti, Ta) borides can be detected. The average grain size of the equiaxed γ-grains is about $7\,\mu m$, and the material is not textured. The density was measured to be $\rho = 4.029 \pm 0.006\,g/cm^3$ which is a higher value than usually reported in literature ($3.7\,g/cm^3 \leqslant \rho \leqslant 3.9\,g/cm^3$). However, the higher density is attributed to the additional Cr-, Nb- and Ta-content. Consequently, the elastic constants were determined as: Young's modulus $E = 168.5 \pm 1.4$ GPa, shear modulus $G = 68.3 \pm 0.3$ GPa and the Poisson's ratio $\nu = 0.23$ (Kauffmann, 1999).

With reference to Eqs. (2.1), (2.7) and (2.13) and the present material (see Fig. 10) the following parameters were taken:

- Taking into account the grain size of the γ-phase the CRSS value for slip $\tau_0^{\alpha} = 130$ MPa has been chosen.
- The same value $\tau_0^{\beta} = 130$ MPa has been taken for deformation twinning.
- Since the contribution of super-dislocations to the deformation behavior of two-phase γ-TiAl based alloys is very small, a high CRSS $\tau_0^{super} = 500$ MPa is chosen.

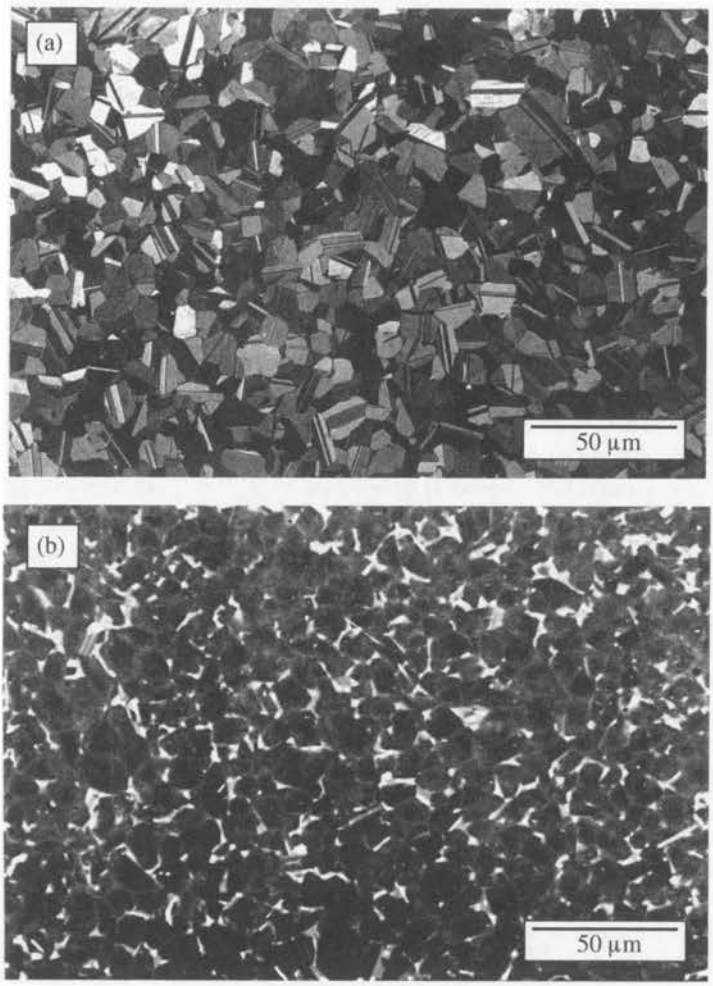

FIGURE 10. Microstructure of as-HIPed Ti-46.5Al-4(Cr,Nb,Ta,B) with near-γ microstructure prior to compression testing. (a) Optical microscopy image, (b) back-scattered electron image. Dark phase: γ-TiAl; light phase: α_2-Ti_3Al; white phase: B2-phase.

- As to the α_2-phase, prism $\{10\bar{1}0\}\langle\bar{1}\bar{2}10\rangle$-, basal $(0001)\langle\bar{1}\bar{2}10\rangle$- and pyramidal $\{11\bar{2}1\}\langle11\bar{2}\bar{6}\rangle$-slip systems can be activated in the α_2-Ti_3Al phase depending on the crystal orientation. The CRSS for pyramidal slip is much higher than that for prism slip and basal slip is also seldom observed due to high CRSS (Umakoshi et al., 1993). Therefore, in our simulations pyramidal and basal slip is neglected while the value of $\tau_0^{\text{prism}} = 260\,\text{MPa}$ for the CRSS of prism-slip is chosen. Applying Eq. (2.13) would give a diameter of $d = 2\,\mu\text{m}$ for the α_2-phase which is in good relation to the microstructure shown in Fig. 10.
- All other parameters which are not influenced by the material properties remain the same as given in the calibration (see above).

2.4. Results and discussion

In Fig. 11a and 11b the predicted and experimentally observed stress-strain curves measured in compression for three different strain rates ($\dot{\varepsilon} = 2 \cdot 10^{-5}\,s^{-1}$, $\dot{\varepsilon} = 2 \cdot 10^{-4}\,s^{-1}$ and $\dot{\varepsilon} = 2 \cdot 10^{-3}\,s^{-1}$, respectively) are shown. It can be seen that the micromechanical model reflects the stress-strain behavior of the material well. However, the model can not capture the plateau-like feature seen in the experimental curve. A similar behavior was observed for fcc-materials with a low stacking fault energy, e.g. polycrystalline Cu-4.9at%Sn, where dislocation glide as well as deformation twinning are the predominant mechanisms during plastic deformation. Initially, deformation twinning and glide dislocation occur on the same (111)-planes, i.e. the dislocations move parallel to the twin interfaces. Therefore, twinning contributes to the deformation but not to hardening (Reed-Hill and Abbaschian, 1994). At the end of this regime with weak hardening, more twin-systems and/or different planes of glide dislocations are activated and interact. This leads to an increase of hardening. As the $L1_0$-structure is strongly related to the fcc-structure the above mentioned effect can also be applied in γ-TiAl.

In Fig. 12 the AE-results corresponding to the stress-strain curves of the first deformation cycle (Fig. 11a) are depicted. The AE-curves show the same characteristic shape for all three applied strain rates. AE starts right after the elastic part in the stress-strain-curve. This is due to plastic deformation in some "favorable" oriented grains (high Schmid-factor), while in other grains still elastic deformation is predominant. A pronounced peak of AE activity is observed in the regime up to 1.0% strain. Beyond the maximum the RMS voltage drops rapidly and stays mostly close to the noise level. The distinct peaks at strains higher than 0.03 result from micro-cracks.

A more distinct observation of the experimental data drawn in Fig. 12 shows that the maximum RMS voltage appears to move to slightly higher strains with increasing strain rate. The maximum of RMS-voltage in the experiment with $\dot{\varepsilon} = 2 \cdot 10^{-5}\,s^{-1}$ is found at a strain of $\varepsilon = 0.0045$, for $\dot{\varepsilon} = 2 \cdot 10^{-4}\,s^{-1}$ at $\varepsilon = 0.0048$ and for $\dot{\varepsilon} = 2 \cdot 10^{-3}\,s^{-1}$ at $\varepsilon = 0.0051$, respectively. As a general observation, one can see that the RMS signal increases with increasing strain rate. This behavior is expected as the level of RMS voltage depends on the number of AE-events per time interval (Hamstad, 1987).

The course of RMS-voltage shows its maximum exactly in the regime of strain, where only weak hardening is observed. This can be interpreted as the first indication for a relationship between acoustic emission and twinning in addition to the following arguments: AE from fracture in the α_2-phase can be excluded since microscopic investigations did not show any cracks in the α_2-phase. Furthermore, this effect could not explain the coincidence of AE and the regime of weak hardening. If we consider dislocation movement as the source of AE, one has to argue that a great number of dislocations (pinned dislocations) move at the beginning of plastic deformation in an avalanche-like way and "run" simultaneously through the material. At a strain of about 1% this effect disappears. In the stress-strain-curve a well developed plateau-like feature as shown in Fig. 11a can be expected. However, compression-experiments on γ-TiAl exhibiting 3 vol% twins already before the AE-testing did not show such a plateau. On the other hand the volume fraction of

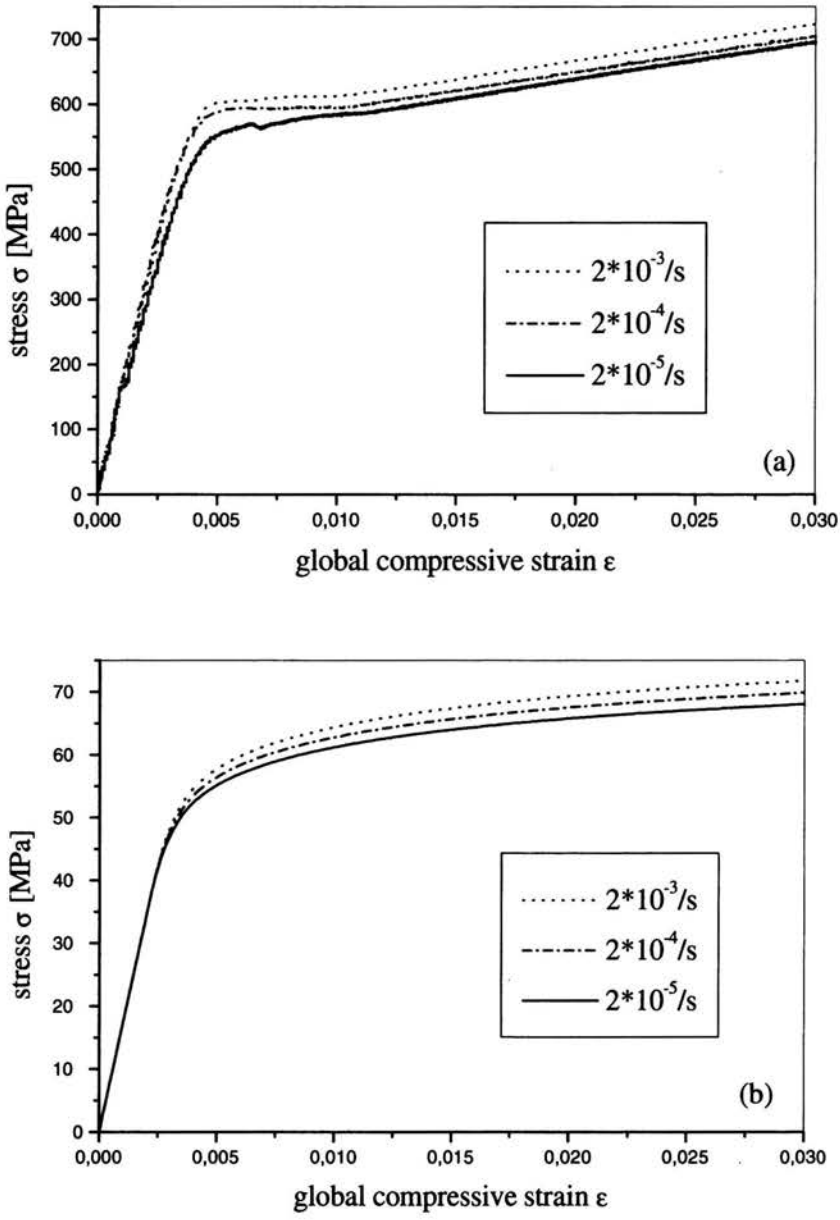

FIGURE 11. Stress-strain curves of a TiAl-based material with near-γ microstructure obtained by uniaxial compression tests applying three different strain rates $\dot{\varepsilon}$. (a) experimental (Ti-46.5at%Al-4at%(Cr, Nb, Ta, B)), (b) predicted by the simulation.

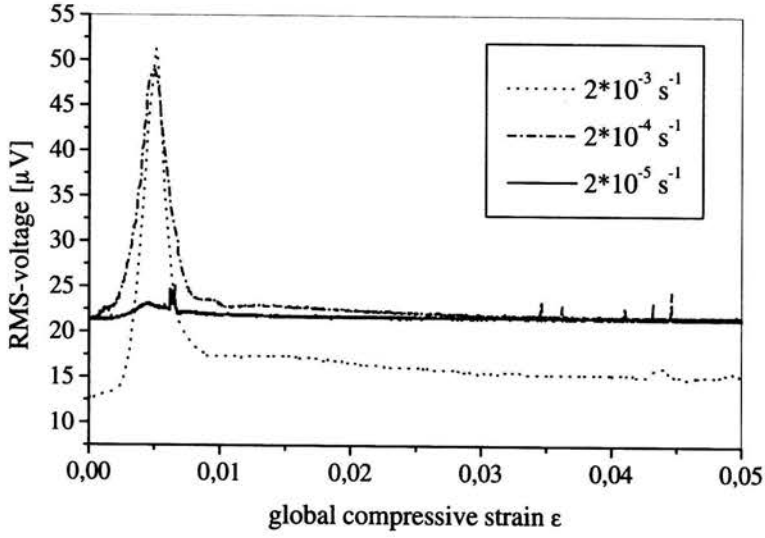

FIGURE 12. Comparison of RMS-voltage in AE measurements applying three different strain rates.

twins increased up to 6% during the compression test, and AE could be detected (Bidlingmaier et al., 1999).

If one compares Fig. 12 with Fig. 11a it can clearly be seen that the region of AE coincides exactly with the plateau-like region (i.e. weak hardening) in the corresponding stress-strain curve. This observation suggests that twinning might be the predominant deformation mechanism at low strains for the reasons given at the beginning of this section. The following experiments were performed (Kauffmann, 1999; Marketz et al., 2001a) to confirm this assumption:

If the material is reloaded immediately after the first deformation cycle, yielding occurs at a stress of ~ 700 MPa, which corresponds to the maximum stress at the end of the first cycle (Fig. 13c). No region of low strain hardening rate can be found, and no AE peak is observed (Fig. 13d). The slight increase of the RMS signal at the start of the second deformation cycle is due to the load-dependent noise from the testing machine.

This experiment with immediate reloading after the first deformation cycle shows a continuation of plastic deformation at the maximum stress level reached during the first cycle (Figs. 13a and 17c). The same result was obtained for a sample aged 4 months at room temperature prior to a second deformation cycle (Kauffmann et al., 2000). Thus, the AE signal is not a result of processes which recover at room temperature.

In case of the specimen being annealed for 2 hours at 800°C after the first deformation cycle and subsequently reloaded, a similar behavior as mentioned above has been observed (Fig. 13). No AE peak occurred, and the stress-strain curves are devoid of a plateau-like region (Figs. 14c and 14d). However, the yield stress is

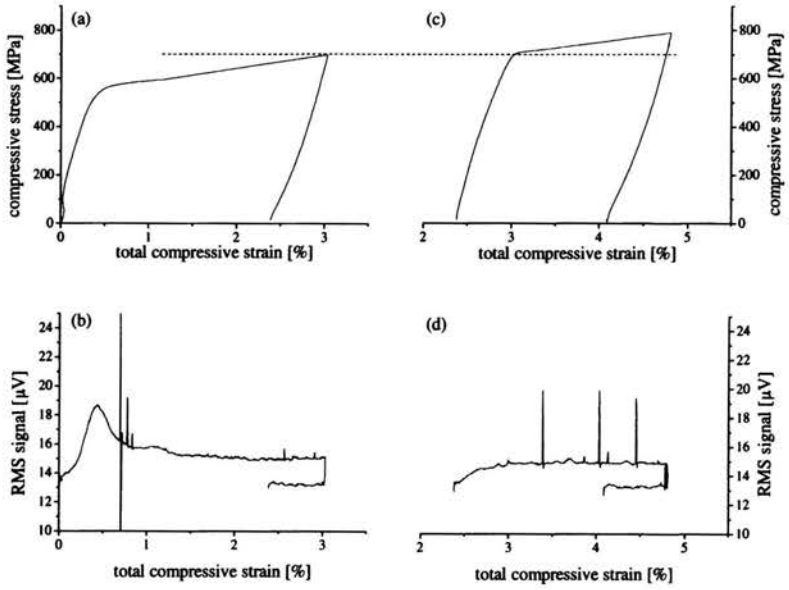

FIGURE 13. Stress-strain curves and the correspondent RMS signal for the first deformation (a and b) and for the second deformation cycle (c and d). The specimen was reloaded without any heat treatments after the first deformation cycle. The spikes in c are due to electromagneti interference, i.e. they are not characteristic for the AE-behavior of the material.

almost as low as that observed in the first cycle (Fig. 14c). One can conclude that annealing at 800°C causes only the yield stress to recover which implies that the dislocation density has decreased, since TEM studies showed that the density of mechanical twins remained unaffected. Although the dislocation density must have been decreased during annealing, no considerable AE activity was detected in the present study during reloading of the specimen. This suggests that dislocation glide gives only a weak contribution to the AE signal.

In contrast, after annealing a deformed specimen for 100 hours at 1000 °C, the yield stress is found to be as low as for the as-processed state and also the AE peak, and the region of weaker strain hardening appears again (Fig. 15c and 15d). This implies that the mechanisms responsible for both effects have recovered during annealing. TEM investigations show a significant decrease in the twin density as a result of the heat treatment. The more pronounced AE activity during deformation of the annealed material is assumed to result from an increase in the γ-TiAl grain size.

Sticking to the assumption that twinning is the source of AE it seems clear that at the beginning a great number of new twins are formed and contribute to the plastic deformation. At higher strains only a few new twins are activated, while the already existing twins inhibit the further twin production and hinder dislocation movement. Further arguments for the latter assumption stem from experiments of other materials with the same experimental setup, where AE from dislocation glide

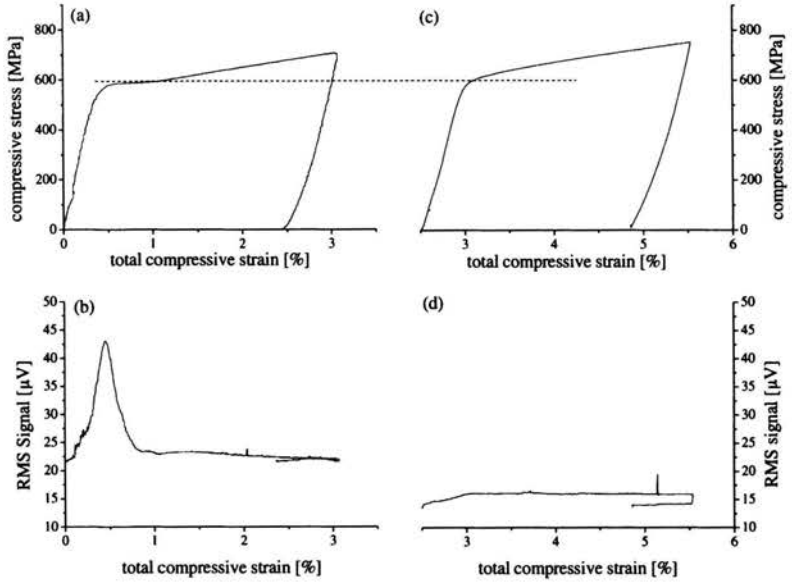

FIGURE 14. Stress-strain curves and the corresponding RMS signals for the first deformation cycle (a and b) and for the second deformation cycle (c and d). The second deformation cycle was performed after annealing the specimen at 800°C for 2 hours.

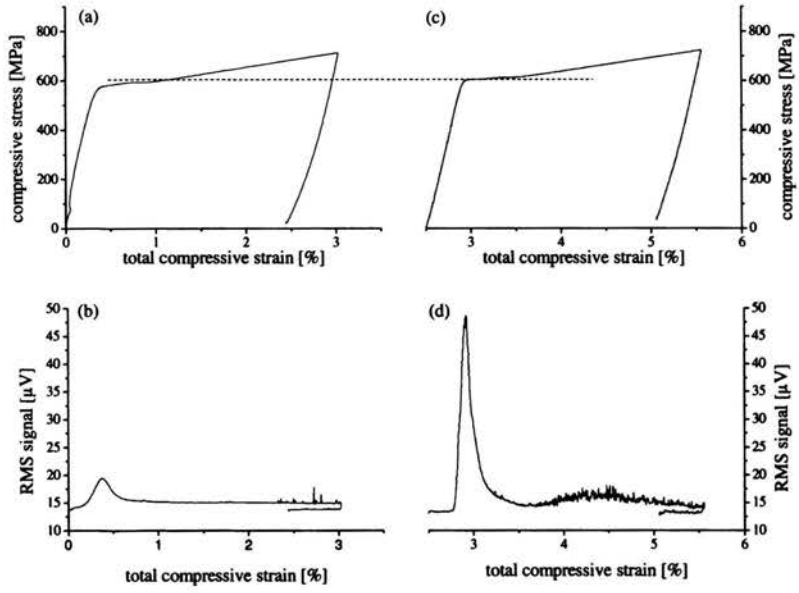

FIGURE 15. Stress-strain curves and the corresponding RMS signals for the first deformation cycle (a and b) and for the second deformation cycle (c and d). The second deformation cycle was performed after annealing the specimen at 1000°C for 100 hours.

could not be observed. On the other hand AE-investigations conducted on Uranium show similar results, and there is no doubt that twinning is the decisive influence (Heiple and Christiansen, 1986).

In contrast, TEM studies of specimens deformed to $\varepsilon = 0.05$ reveal a large number of twins, indicating that mechanical twinning is an important mechanism of plastic deformation in γ-TiAl. Additionally, a significant increase in dislocation density is observed (Kauffmann et al, 2000).

From the above given results the following interpretation can be concluded:

> In case of annealing at 1000°C for 100 hours after a first deformation cycle, the deformation twin density decreased significantly mainly due to static recrystallization. Twins which are formed in the recrystallized coarse grains are able to expand over larger distances than in the finer-grained initial material (Reed-Hill and Abbaschian, 1994). Therefore, more energy is released per mechanical twin, which leads to increased AE signals. Another possibility to explain the increased AE peak height is that the ratio of dislocation glide to mechanical twinning in the larger grains is shifted towards the twinning mechanism, because a higher Hall-Petch constant is expected for the twinning process than for the dislocation glide process. This means that with increasing grain size the stress necessary for twinning decreases faster than that for gliding. As the AE characteristics is affected by the grain size in several ways (Heiple and Carpenter, 1987; Heiple and Christiansen, 1986) the pronounced increase of AE due to the intermediate heat treatment cannot be related to a specific mechanism. However, the experiments performed on the differently annealed specimens show clearly that the AE is caused by the formation of mechanical twins. In addition, the onset of AE coincides well with the onset of twin deformation as predicted by micromechanical simulations (Marketz et al., 2000).

The observed plateau-like region adjacent to the elastic regime is reported to occur for materials which deform by both mechanisms, namely dislocation glide and deformation twinning. When plastic deformations at low strains lead to dislocation glide and twinning on the same (111) planes, both mechanisms contribute to the total strain but not to strain hardening. With increasing strain more and more twinning systems are activated, which have different twin planes and are hence in the position to interfere with the gliding dislocations and thus contribute to strain hardening (Reed-Hill and Abbaschian, 1994).

This kind of behavior has earlier been observed in copper, which shows with its fcc crystal structure and its low stacking fault energy a similar deformation behavior as the tetragonal face centered γ-TiAl phase (c/a-ratio 1.02) investigated here.

The results obtained in this study and the correlation of deformation twinning with the AE signal allow an explanation of the course of the AE activity with deformation. The twins nucleate predominantly at the beginning of plastic deformation. There are indications that in this regime deformation is mainly carried by mechanical twinning of favorably orientated grains. With increasing strain, however, deformation is more and more dominated by the movement of dislocations. Furthermore, the primary twin system limits the propagation of further twin systems due

to the formation of twin intersections. Both mechanisms give a natural explanation for the decay of the AE at $\sim 0.5\%$ total compressive strain.

In the following Fig. 16 TEM micrographs of the virgin material and of the deformed material are depicted. One can recognize that the starting material exhibits no twins while in the deformed configuration ($\varepsilon = 0.05$, $\dot{\varepsilon} = 2 \cdot 10^{-4} s^{-1}$) a high twin density of two different twin systems occurs.

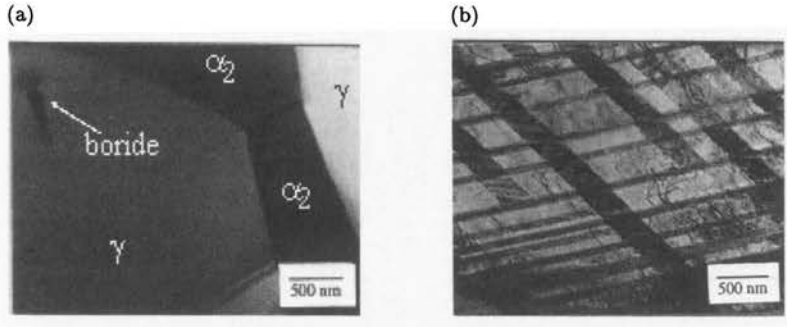

FIGURE 16. (a) TEM image revealing the microstructure of an undeformed sample. Additionally, (Ti,Ta)-borides (B) are embedded in γ-grains as detected by TEM. The deformed sample (b) shows mechanical twins with two different orientations and dislocations ($\varepsilon = 0.05$, $\dot{\varepsilon} = 2 \cdot 10^{-4} s^{-1}$).

Based on our description of twinning, the presented micromechanical model allows to find the value of the global strain where twinning occurs as a deformation mechanism. A different onset of twinning as well as a different evolution of the twin volume fraction in each grain can be seen in Fig. 17. These simulation results match

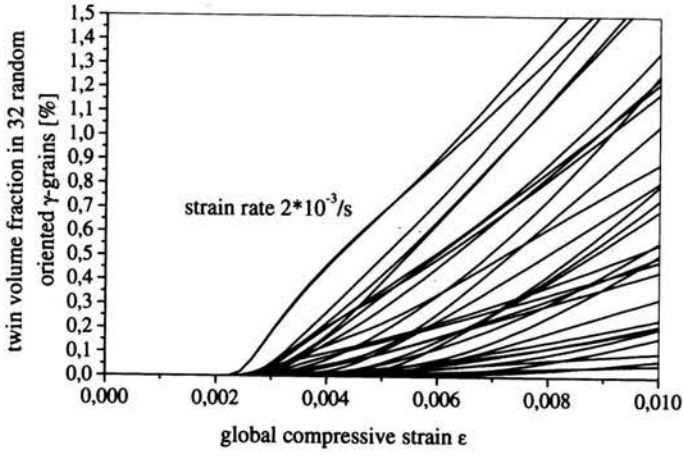

FIGURE 17. Twin volume fraction in each of the 32 randomly oriented γ-grains as a function of the global compressive strain.

well with an experimental TEM study, where the volume fraction of mechanical twins within a randomly chosen grain after a global deformation of $\varepsilon = 0.006$ was determined (Kauffmann et al., 2000). This is obviously due to the different Schmid-factors for slip and twinning which depend on grain orientation. Further simulations did not show any strain rate dependence of the onset of twinning, but the contribution of twinning to the total deformation is higher in the case of a

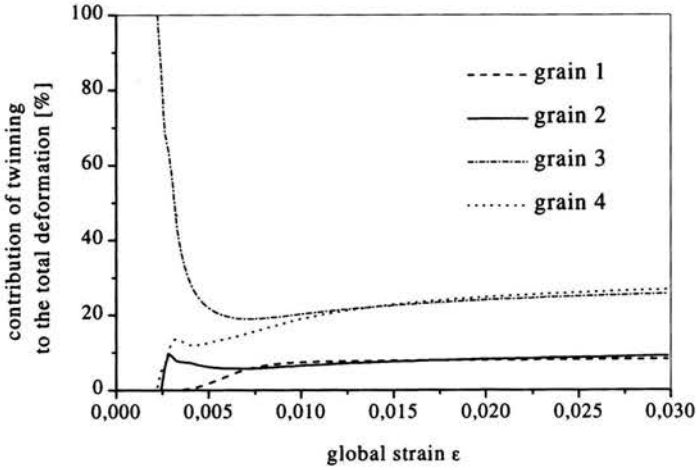

FIGURE 18. Contribution of twinning to the total plastic deformation depicted exemplary for four γ-grains in a uniaxial tension test applying a strain rate of $2 \cdot 10^{-3}\,s^{-1}$.

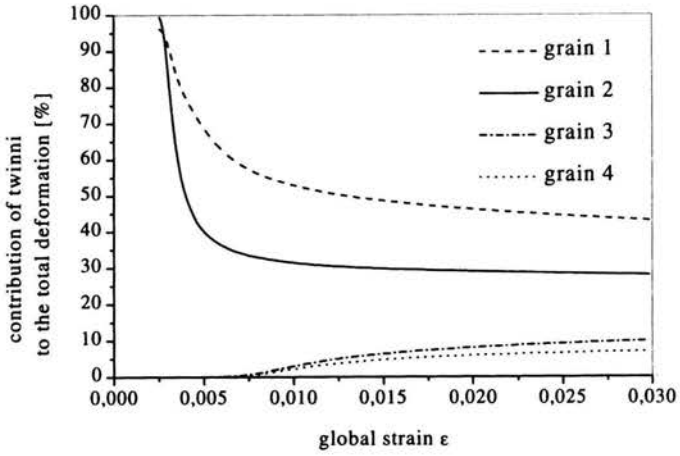

FIGURE 19. Contribution of twinning to the total plastic deformation depicted exemplary for four γ-grains in a uniaxial compression test applying a strain rate of $2 \cdot 10^{-3}\,s^{-1}$. The grains are the same as in the tension test according to Fig. 18.

smaller strain rate. This fact could explain the shift of the AE maximum to higher strains with higher strain rates.

Figure 18 shows the contribution of twinning to the total plastic deformation in four different oriented γ-grains during a uniaxial tension test at a strain rate of $2 \cdot 10^{-3}\,s^{-1}$. That contribution depends on the lattice orientation of the grain with respect to the load axis. In some grains twinning appears to be the major deformation mechanism at lower strains ($0.002 \langle \varepsilon \langle 0.02$) until the ratio twin-contribution/slip-contribution reaches a constant value at higher strains ($\varepsilon > 0.02$). In comparison, Fig. 19 shows the contribution of twinning to the total plastic deformation in the same four γ-grains in an uniaxial compression test at the same strain rate. The unidirectionality of twinning is clearly demonstrated, and one can see the importance of the different deformation mechanisms depending on the load case.

3. Creep of γ-TiAl based alloys – computational modelling based on experimental investigations

It is well known that the mechanical properties of γ-TiAl alloys depend strongly on microstructure, which in turn is influenced by the alloy chemistry and the applied heat treatments. A designed fully lamellar (DFL) microstructure which consists of colonies of parallel γ-TiAl (tetragonal face centered $L1_0$ structure) and α_2-Ti_3Al (ordered hexagonal DO_{19} structure) laths with a colony size in the range of 150-200 μm possesses superior creep resistance. Recent studies (Parthasarathy et al., 1998; Crofts et al., 1996; Maruyama et al., 1997) have shown that interface spacing influences the creep behavior. This allows the conclusion that the interfaces γ/γ and α_2/γ must play a role in limiting creep flow or providing creep strength.

Differently spaced DFL microstructures were adjusted in order to investigate their influence on creep. Fine grained sheet material exhibiting a nominal composition of Ti-46.5at%Al-4at%(Cr,Nb,Ta,B) was used, and short term creep tests were carried out in air at 700°C and 800°C under a load stress of 175 MPa constant in time. The interface spacing was varied in the range of 1.2 μm to 0.14 μm by altering the cooling rates from 1 K/min to 200 K/min. An approach in modelling the steady state creep deformation of the fully lamellar material in question is presented. A power law description for diffusion controlled dislocation creep is proposed, and a structure factor is introduced which depends on the lamellar orientation with respect to the loading axis as well as on the mean lamellar interface spacing.

3.1. Material and experimental

The experimental investigations were conducted within the framework of a close cooperation between the Institute of Mechanics in Leoben, the Institut für Metallkunde in Stuttgart and the above mentioned Max-Planck-Institut für Metallforschung in Stuttgart (Marketz et al., 2001b).

The lamellar structure of a single grain is formed according to the orientation relationships $\{111\}_\gamma \parallel (0001)\alpha_2$ and $\langle 110\rangle_\gamma \parallel \langle 11\bar{2}0\rangle\alpha_2$. As a consequence, six different types of ordered domains exist in the γ-phase within the lamellar structure (Inui et al., 1992), i.e. the matrix domains I (γ^1), II (γ^2) and III (γ^3), and the twin domains I, II and III (γ^4, γ^5 and γ^6). A good tool for studying the effects of the

lamellar structure is provided by so called polysynthetically twinned (PST) single crystals (Fujiwara et al., 1990).

In this study the investigated sheet material with a nominal composition of Ti-46.5at% Al-4at%(Cr,Nb,Ta,B) was fabricated at Plansee AG, Austria, by a powder metallurgical process followed by rolling. A detailed description of the rolling process is reported by Clemens et al., 1997. A subsequent heat treatment at 1000°C for 2h delivered the starting material exhibiting a primary annealed (PA) microstructure. The PA microstructure predominantly consists of equiaxed γ-TiAl grains with an average grain diameter of 15-20 μm and approximately 5 vol% of $\alpha_2 Ti_3Al$ phase located at grain boundaries and triple junctions of γ-grains. Creep test specimens with an overall length of 50 mm and a gauge area of 30 mm × 3 mm (thickness 1 mm) were cut from the PA sheet material by spark erosion parallel to the rolling direction. In order to obtain a so-called designed fully lamellar (DFL) microstructure the specimens were heat-treated at 1350°C, which corresponds to a temperature above the α-transus temperature of the alloy. Differently spaced lamellae were obtained by varying the cooling rates. Figure 20 demonstrates the course of the heat treatments schematically.

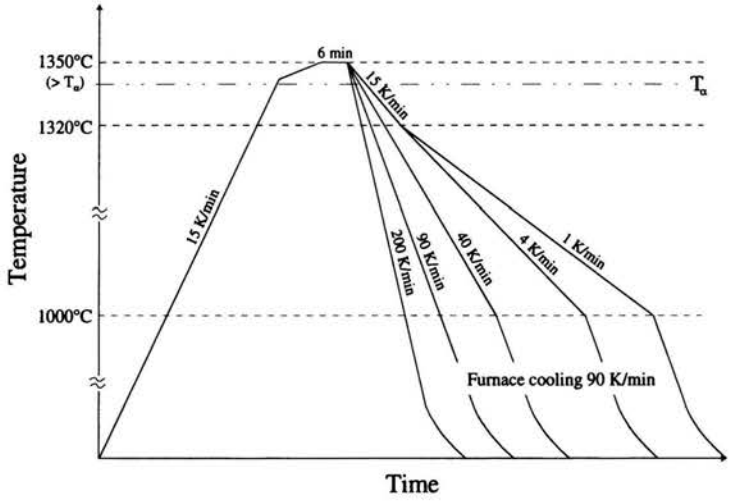

FIGURE 20. Schematic drawing of the heat treatment resulting in microstructures with different lamellar spacing but comparable colony size.

After a certain hold time at 1350°C the samples were cooled with 15 K/min below the α-transus temperature. This step was performed to prevent possible grain growth within the α-transus field, thus to achieve comparable colony sizes. Subsequently, the specimens were cooled to 1000°C applying different cooling rates. This results in the formation of different mean interface spacings. After reaching 1000°C the specimens were cooled to room temperature by furnace cooling. The highest cooling rate (200 K/min) was obtained by floating with argon.

The creep samples were tested in tension in air at 700°C and 800°C and a constant load, which corresponded to a constant load stress of 175 MPa. In order to

investigate the microstructure developing during deformation within the secondary creep regime by transmission electron microscopy (TEM), the tests were interrupted at a strain of approximately 2.5%. To preserve the creep microstructure the specimens were cooled down to room temperature under applied load.

Optical microscopy under polarized light was used to determine the mean colony size by using the linear intercept method. The mean interface spacing of "edge on" tilted colonies was measured by TEM. At least 200 to 400 laths were considered, and no distinction was made between α_2/γ and γ/γ interfaces.

3.2. Experimental evidence

3.2.1. Microstructure. The heat-treatments mentioned above have resulted in lamellar microstructures with a mean colony size of 130 μm. The light optical micrographs of three representative specimens which were cooled with 1 K/min, 40 K/min and 200 K/min, respectively, are shown in Fig. 21. While the colony size of all specimens remained similar, the mean interface spacing decreased from 1.2 μm to 0.14 μm with decreasing cooling rate. Metallographic examinations of differently cooled specimens have shown an almost undisturbed fully lamellar microstructure for cooling rates in the range of 4 K/min and 200 K/min. Typical defects such as primary γ-grains at colony boundaries occur with cooling rates < 4 K/min. Cooling rates higher than 200 K/min lead to the appearance of Widmannstätten-like features (Chatterjee et al., 2000).

The lamellar microstructure of specimens cooled within 4-200 K/min consists of regular patterns of alternate α_2 and γ lamellae, as shown in Fig. 21. The mean interface spacing, including α_2/γ and γ/γ interfaces, was found to decrease with increasing cooling rate. The correlation between the mean interface spacing λ [μm] and the cooling rate R_c [K/min] is depicted in Fig. 22 and can be expressed by a fit as

$$\lambda = 1.18\, R_c^{-0.39}. \tag{3.1}$$

3.2.2. Creep behavior. Heat-treated creep specimens with different mean interface spacings but comparable colony size were tested at 700°C and 800°C applying a constant load stress of 175 MPa with the loading axis parallel to the rolling direction. The creep test results obtained for differently spaced DFL microstructures at 800°C are summarized in Fig. 23. All creep tests were carried out to the secondary creep regime. The minimum creep rate decreases significantly with decreasing interface spacing. The correlation between the minimum creep rate $\dot{\varepsilon}_{\min}$ [s^{-1}] and the mean interface spacing λ [μm] at the creep conditions described above can be expressed as

$$\dot{\varepsilon}_{\min}(700°C) = 1.59 \cdot 10^{-9}\, \lambda^{0.68}, \tag{3.2}$$

$$\dot{\varepsilon}_{\min}(800°C) = 1.03 \cdot 10^{-7}\, \lambda^{0.66}. \tag{3.3}$$

An activation energy of $Q = 350$ kJ/mol, which is independent of the mean lamellar spacing, has been determined within the temperature range of 700°C to 800°C and a stress of 175 MPa.

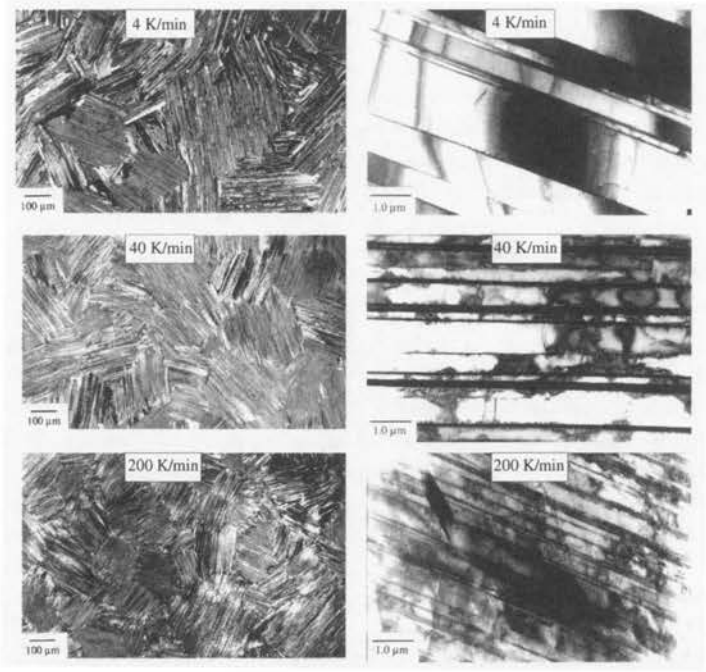

FIGURE 21. Colony size (light optical micrographs) and lamellar spacing (TEM micrographs) obtained in Ti-46.5at%Al-4at%(Cr,Nb,Ta,B) sheet specimens which were annealed at 1350°C for 6 minutes and subsequently cooled with different cooling rates: (a, b) 4 K/min, (c, d) 40 K/min, (e, f) 200 K/min.

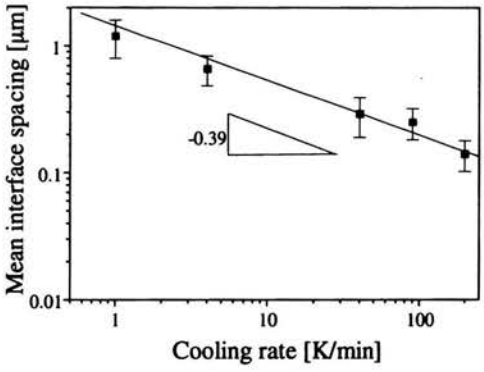

FIGURE 22. Dependence of the mean interface spacing λ on cooling rate R_c obtained for Ti-46.5at% Al-4at%(Cr,Nb,Ta,B) sheet material.

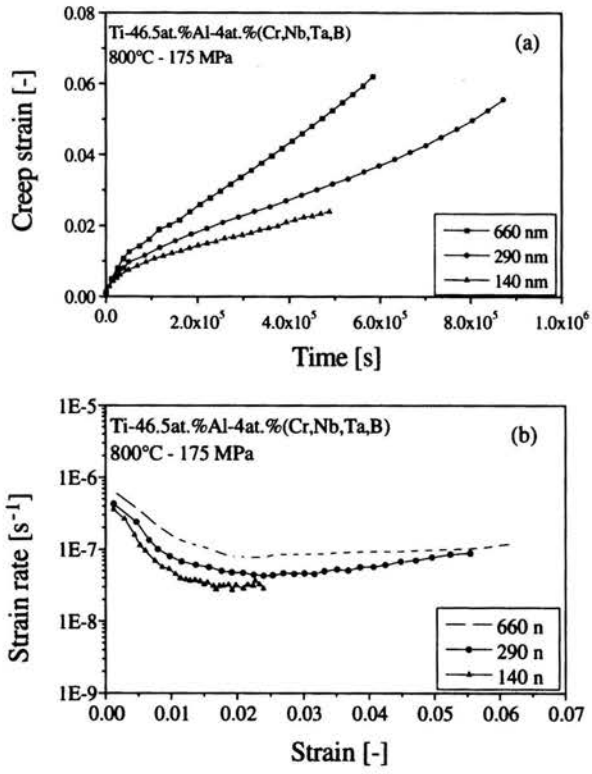

FIGURE 23. Creep behavior of Ti-46.5at% Al-4at%(Cr,Nb,Ta,B) sheet material tested at 800°C and 175 MPa. (a) strain ε vs. time, (b) strain rate $\dot{\varepsilon}$ vs. strain ε.

3.2.3. Experimental evidence. The experimental results point out the significant effect of lamellar spacing in fully lamellar microstructures on the creep behavior of the alloy at the investigated temperatures of 700°C and 800°C under a constant load stress of 175 MPa in terms of minimum creep strain rate. The enhanced creep resistance in terms of decreasing minimum creep rates with the decrease of the lamellar spacing observed in the present study is in accordance with the results reported by Parthasarathy et al., 1998, and Maruyama, 1997. A similar correlation between secondary strain rate and mean interface spacing (Eqs. (3.2) and (3.3)) is also reported by Parthasarathy et al., 1998. However, it is argued that substructure invariant models discussed for dispersion strengthened materials as well as power law creep models are inapplicable to fully lamellar alloys.

In general, two mechanisms are suggested to be responsible for the improvement of creep behavior due to reduced mean interface spacing as shown in Fig. 23a. The first mechanism is the impediment of dislocation glide by a reduced interface spacing. The second mechanism is based on the assumption that the lamellar interfaces restrict dislocation motion parallel to α_2/γ lamellae causing a bowing out of dislocation segments (e.g. see also Wang et al., 1995). TEM investigations conducted on

fully lamellar Ti-46.5at%Al-4at%(Cr,Nb,Ta,B) sheet material confirm both mechanisms. These observations have shown frequent interceptions across γ-lamellae due to the formation of small angle grain boundaries and dislocation pile-ups as well as the formation of subgrain boundaries within γ-lamellae. Furthermore, the formation and emission of dislocation loops as well as the bowing out of dislocations segments between the interfaces were observed. Similar results were found by Chen et al., 1999, who recently reported dislocation bowing between lamellar interfaces of the soft oriented grains, resulting in the assumption that the strain rate of soft grains obeys a power law relation.

3.3. Micromechanical modelling

As indicated in the previous section there are contradictory statements reported in the literature as to whether a power law description of creep of fully lamellar TiAl-materials is applicable. Therefore, the purpose of our computational modelling is a first approach to investigate the application of a power law creep model to describe the creep behavior of DFL γ-TiAl materials.

For many pure metals and alloys an established, largely phenomenological, relationship exists between the steady state strain rate, $\dot{\varepsilon}_{ss}$, and the stress σ, as

$$\dot{\varepsilon}_{ss} = A \exp\left\{-\frac{Q}{RT}\right\} \sigma^n, \tag{3.4}$$

where A is a structure factor, Q is the activation energy for creep, R is the gas constant, T is the temperature and n denotes the stress exponent.

It seems obvious that such a general relation like type (3.4) should fail in the description of the creep behavior of fully lamellar microstructures consisting of differently oriented colonies of α_2- and γ-laths. Furthermore, the creep behavior of the hexagonal α_2-Ti_3Al phase differs from the creep behavior of the tetragonal face centered γ-phase (Bartholomeusz et al., 1993). The effects of the lamellar structure can best be studied with so called polysynthetically twinned (PST) crystals of TiAl. These are single-crystals with lamellar structure (Fujiwara et al., 1990). A detailed investigation of the creep behavior of PST TiAl at 877°C and 200 MPa has been reported by Wegmann et al., 2000. It has been shown that PST orientations with their lamellae parallel or perpendicular to the loading axis (hard mode orientations) exhibit longer creep lives and lower minimum creep rates than soft oriented PST specimens. The hard PST orientation deforms mainly by deformation modes oblique to the lamellar interfaces, whereas the soft orientation deforms mainly by slip parallel to the lamellar interfaces. The effect of the lamellar orientation on the creep resistance is discussed on the basis of the resolved shear stress for ordinary glide dislocations. Due to the fact that the γ-phase is considerably weaker than the α_2-phase at high temperatures the creep resistance is expected to be controlled by the deformation of the γ-constituent. A detailed information on hard- and soft-mode deformation of PST TiAl single-crystals is given by Inui et al., 1995.

3.3.1. Modelling of the creep behavior of single crystal PST TiAl. Based on the above mentioned experimental results and Eq. (3.4) we suggest to modify the latter relation in order to take the lamellar orientation as well as the lamellar

interface spacing of the γ-phase into account. The DFL TiAl investigated does not show an extended steady state creep region but only a minimum creep strain rate. Consequently, the notation $\dot{\varepsilon}_{ss}$ in Eq. (3.4) changes to $\dot{\varepsilon}_{\min}$ in the following. Equation (3.5) gives a new relation between the minimum creep strain rate $\dot{\varepsilon}_{\min}$, temperature T, activation energy Q and applied stress introducing a structure factor $B^{\gamma}(\phi, \lambda)$ depending on the angle ϕ between lamellae orientation and load axis and on the mean interface spacing of the lamellae, respectively. Therefore, the creep behavior, i.e. the minimum creep strain rate $\dot{\varepsilon}^{\gamma}_{\min}$ of the γ-TiAl constituent can be expressed as

$$\dot{\varepsilon}^{\gamma}_{\min} = B^{\gamma}(\phi, \lambda) \exp\left\{-\frac{Q_{\gamma}}{RT}\right\} \sigma^{n_{\gamma}}. \tag{3.5}$$

The index γ stands for the activation energy Q and the stress exponent in the γ-TiAl phase, whereas Q_{α} is the activation energy and n_{α} is the stress exponent in the α_2-Ti_3Al phase. Consequently, the creep behavior of the α_2-phase is described by a relation

$$\dot{\varepsilon}^{\alpha}_{\min} = B^{\alpha} \exp\left\{-\frac{Q_{\alpha}}{RT}\right\} \sigma^{n_{\alpha}}. \tag{3.6}$$

The input data for our modelling are taken from literature available for single α_2-Ti_3Al phase and single γ-TiAl phase without additional alloying elements (Bartholomeusz et al., 1993; Es-Souni et al., 1993; He et al., 1997, Schafrik, 1977). The elastic constants, the activation energy and the stress exponent for both phases at 800°C are given in Table 4. For a first approach the structure factor B^{α} for the α_2-phase is assumed to be independent of lamellae orientation and lamellae thickness. This assumption seems to be justified since the volume content of the α_2-phase is lower than 10 vol%. The value is calculated from experiments by Bartholomeusz et al., 1993) to be $B^{\alpha} = 5.49 \cdot 10^{14}\,\mathrm{GPa}^{-n}\,\mathrm{s}^{-1}$.

TABLE 4. Elastic constants, activation energy and stress exponents for γ-TiAl- and α_2-Ti_3Al single phase materials.

Material	E(800°C)	ν(800°C)	Activation energy Q	Stress exponent n
γ-TiAl	102.0 GPa	0.28	380 kJ/mol	7.2
α_2-Ti_3Al	150.0 GPa	0.247	352 kJ/mol	5.5

The activation energy for γ-TiAl is taken from creep experiments conducted on fine-grained Ti-46.5at% Al-4at%(Cr,Nb,Ta,B) sheet with near gamma microstructure. The stress exponent of n=7.2 for γ-TiAl indicates that the creep process is mainly determined by dislocation glide and dislocation climb. Simulations with the orthotropic elasticity tensor for TiAl and Ti_3Al did not show any significant difference in the results compared to cases, where isotropic elasticity in each constituting phase is assumed.

3.3.2. Determination of the structure factor $B^{\gamma}(\phi, \lambda)$. To determine the structure factor $B^{\gamma}(\phi,\lambda)$ we fit our model to the experimental data obtained by

Wegmann et al., 2000. The nominal composition of the PST TiAl crystal used in their study was binary Ti-48at%Al.

The arrangement of the ordered γ-domains between the α_2-lamellae can be seen in Fig. 24. A three-dimensional FE model is chosen for the simulations of PST crystals in this work. The RVE represents the microstructure and the behavior of

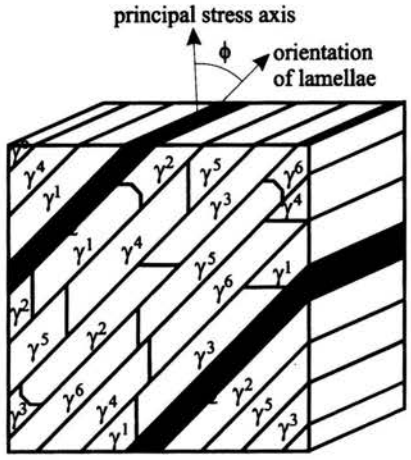

FIGURE 24. Three-dimensional unit cell representing the lamellar microstructure of a PST crystal formed of six ordered domains of γ-TiAl and 10 vol% of α_2-Ti_3Al, after Schlögl and Fischer, 1997.

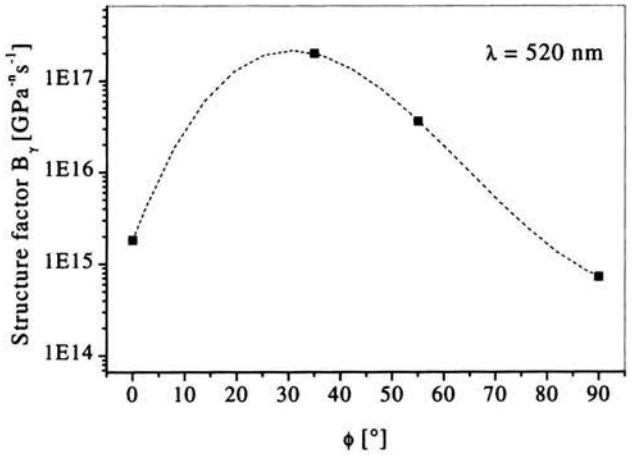

FIGURE 25. Dependence of the structure factor B^γ on the orientation angle ϕ between the lamellae and the loading axis. The dashed line indicates a polynomial fit to B^γ obtained for four orientations ϕ.

the whole specimen. The orientation angle ϕ is determined by the length/height ratio of the unit cell. An amount of 10 vol% of α_2-Ti_3Al and all six ordered domains of the γ-phase are considered. The selected orientations of the lamellae relative to the load axis are taken from literature (Wegmann et al., 2000) as well as the dimensions of the specimen. A periodic arrangement of a set of unit cells represents a great number of parallel α_2-Ti_3Al and γ-TiAl lamellae by applying periodic boundary conditions which ensure periodicity. The field equations are solved applying the finite element package ABAQUS.

In Fig. 25 the dependence of the structure factor B^γ on the orientation of the lamellae at a fixed mean interface spacing of $\lambda = 520\,\text{nm}$ is depicted ($B^\gamma \rightarrow B^\gamma(\phi, \lambda = 520\,\text{nm})$). For our further simulations we assume that the relationship of $B^\gamma(\phi)$ obtained for Ti-48at%Al PST crystals is the same as in the polycrystalline Ti-46.5at%Al-4at%(Cr,Nb,Ta,B) material with DFL microstructure that we investigated.

3.3.3. Modelling of the creep behavior of polycrystalline TiAl with fully lamellar microstructure. In order to simulate the creep behavior of a DFL polycrystal with different mean interface spacings the dependence of the structure factor B^γ on the interface spacing at a fixed orientation angle ϕ is needed additionally. From the experimental results (Fig. 23) and Eqs. (3.2) and (3.3) we infer the following relation with w given in Eq. (3.2) for 700°C and Eq. (3.3) for 800°C. The constant c and the function $f(\phi)$ are obtained from the experiment.

The major difficulty inherently associated with the modelling of a lamellar polycrystal is to find a RVE just large enough to represent the entire material sufficiently well, and, on the other hand, as small as possible in order to keep the computational effort low. In our case the microstructure is assumed to show periodic patterns with different oriented lamellar colonies. The developed RVE for the DFL microstruc-

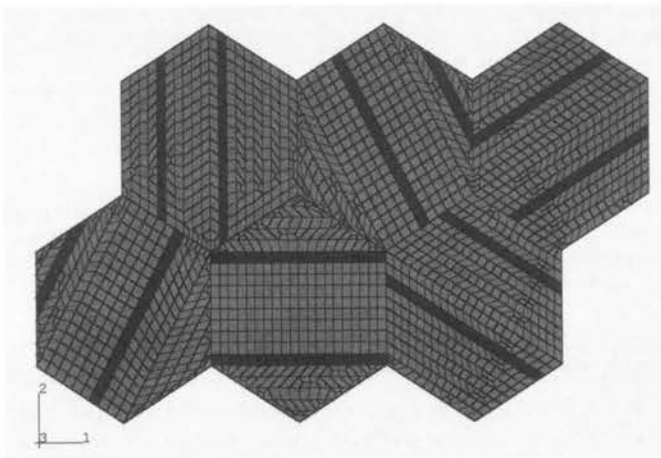

FIGURE 26. Finite element mesh for the DFL microstructure. The α_2-laths are indicated by the darker shading. All six grains exhibit a different orientation of the γ- and α_2-lamellae.

ture exhibits six hexagonal grains with different orientation of the lamellae and is depicted in Fig. 26. The finite element mesh consists of 2085 6-node bilinear quadrilateral generalized plane strain elements. Appropriate periodic boundary conditions are applied to the edges of the RVE and

$$\frac{B^{\gamma}(\phi,\lambda)}{\lambda^{w}} = c\, f(\phi). \tag{3.7}$$

3.4. Results and discussion

Using Eqs. (3.5), (3.6) and (3.7) to describe creep properties for the individual phases, we can compute the global creep deformation behavior of the DFL microstructure applying our FE-model. Several orientations and mean lamellar interface spacings were studied for the DFL microstructure. Figure 27 shows the dependence of the minimum creep rate $\dot{\varepsilon}_{\min}$ on the mean lamellar interface spacing at $T = 700°C$ and $T = 800°C$ under a load stress of $\sigma = 175\,\text{MPa}$ obtained experimentally and by simulation, respectively.

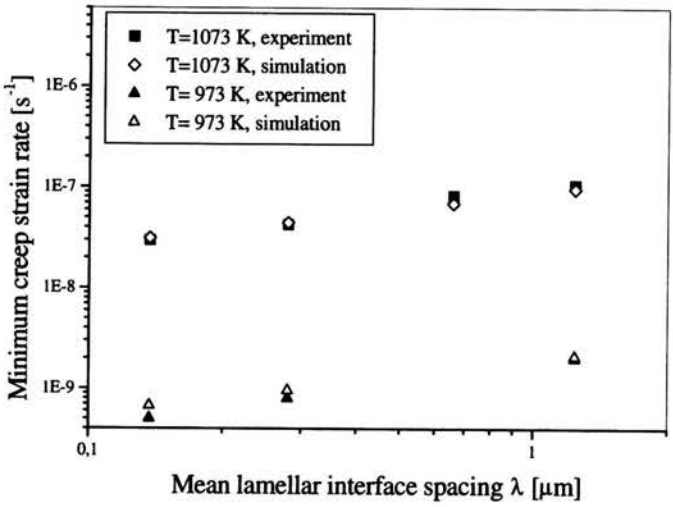

FIGURE 27. Minimum creep rate $\dot{\varepsilon}_{\min}$ as a function of the mean lamellar interface spacing λ at temperatures of 700°C and 800°C and a constant load of 175 MPa. Calculated data (open symbols) and experimental data (solid symbols) obtained on Ti-46.5at% Al-4at%(Cr,Nb,Ta,B) material with DFL microstructure (colony size $\sim 130\,\mu\text{m}$).

In our micromechanical model, the DFL microstructure is composed of a number of differently oriented lamellar single crystals. We introduced a structure factor B which depends on the lamellar orientation ϕ and the mean lamellar interface spacing λ. $B^{\gamma}(\phi,\lambda)$ was determined for each colony orientation as well as for different lamellar spacings from creep data obtained on PST single crystals. The FE simulations match quite well with the experimental data for temperatures of 700°C and 800°C. However, further research is necessary to extent the finite element model

for other creep mechanisms occurring under different creep conditions. One limiting factor that still remains is the availability of experimental data of the single constituent phases, such as the stress exponent at lower temperatures. Finally, the role of additional alloying elements, i.e. Cr, Nb, Ta in our investigated material has to be studied and considered in the model.

Moreover, the dependence of the exponent w in Eq. (3.7) on temperature, prevailing creep mechanism and content of alloying elements has to be studied. Depending on the cooling rate the average interface spacing of a Ti-46.5at% Al-4at%(Cr,Nb,Ta,B) material, as measured by TEM, varied between 0.14 μm and 1.2 μm for fully lamellar microstructures with comparable colony sizes. Creep tests conducted at 700°C and 800°C under a constant load stress of 175 MPa indicated that the minimum creep rate decreases monotonically with decreasing interface spacing. Creep tests performed on this sheet material with DFL microstructure did not show any grain boundary sliding, and the main creep deformation mechanism under the given conditions appeared to be diffusion controlled dislocation creep. A first approach in computational modelling simulation confirmed that a power law creep model can describe the creep behavior of DFL microstructures in the range of 700°C to 800°C if a structure factor depending on the lamellar orientations and the mean lamellar interface spacing is introduced.

4. Summary and outlook

The present work dealing with the micromechanical modelling of the deformation behavior of γ-TiAl based alloys is the result of a strong interplay of numerical simulation and detailed experimental investigations. The main goal of these studies have been the improvement and the extension of a previously developed micromechanical model [35, 42] in order to describe the deformation behavior of polycrystalline materials. The combination of experimental and computational investigations has always been based on the basic idea to enrich one scientific method by the other and vice versa.

In the first part of the studies a micromechanical model describing the deformation behavior of a γ-TiAl-based alloy exhibiting an equiaxed near-γ microstructure is presented. The global stress strain behavior of the untextured Ti-46.5at%Al-4at%(Cr,Nb,Ta, B) alloy is simulated and compared with results from mechanical tests. The model takes crystallographic slip and mechanical twinning into account. Simulations and experiments of compression tests and tensile tests applying different strain rates match well with respect to the global stress-strain curves as well as the onset of mechanical twinning. Accompanying acoustic emission measurements suggest that twinning is the major deformation mechanism in the strain regime lower than 2% of plastic strain. The model also predicts the twin volume fraction in the γ-grains and works out the importance of twinning as a major deformation mechanism in the γ-phase, which is in agreement with TEM studies.

The interest of further activities in the micromechanical modelling should be addressed to extend the present user material subroutine to implement a discrete twin structure. With respect to the nucleation of a twin and the final twin width energy based analytical and numerical studies following the work of Petryk, 1992,

have already been started and are supposed to be very promising. A further important subject is to investigate the influence of additional ternary elements on the deformation behavior of γ-TiAl based alloys.

In the second part of the work the creep behavior of a designed fully lamellar (DFL) γ-TiAl alloy has been investigated. Depending on the cooling rate the average interface spacing of a Ti-46.5at% Al-4at%(Cr,Nb,Ta,B) material, as measured by TEM, varied between 0.14 μm and 1.2 μm for fully lamellar microstructures with comparable colony sizes. Creep tests conducted at 700°C and 800°C under a constant load stress of 175 MPa indicated that the minimum creep rate decreases monotonically with decreasing interface spacing. Creep tests performed on this sheet material with DFL microstructure did not show any grain boundary sliding and the main creep deformation mechanism under the given conditions appeared to be diffusion controlled dislocation creep. A first approach in computational modelling simulation confirmed that a power law creep model can describe the creep behavior of DFL microstructures if a structure factor depending on the lamellar orientations and the mean lamellar interface spacing is introduced. The results of this combined experimental and numerical studies have been very promising, however, further research is necessary to extent the finite element model for other creep mechanisms occurring under different creep conditions. In this respect the microstructural stability of the alloy plays an important role.

Acknowledgement

The authors appreciate the funding by FWF and OeNB under the project number 491/P12418-TEC.

References

1. Y.-W. KIM, Ordered intermetallic alloy, Part III: Gamma titanium aluminides, *JOM*, Vol.46, pp.30-39, 1994.

2. Y.-W. KIM, Intermetallic alloys based on gamma titanium aluminide, *JOM*, Vol.41, pp.24-30, 1989.

3. Y.-W. KIM and D.M. DIMIDUK, Progress in the understanding of gamma titanium aluminides, *JOM*, Vol.43, pp.40-47, 1991.

4. H. CLEMENS, Intermetallic γ-TiAl based alloy sheet materials - processing and mechanical properties, *Z. Metallkd.*, Vol.86, pp.814-822, 1995.

5. H. CLEMENS, A. LORICH, N. EBERHARDT, W. GLATZ, W. KNABL and H. KESTLER, Technology, properties and applications of intermetallic γ-TiAl based alloys, *Z. Metallkd.*, Vol.90, pp.569-580, 1999.

6. P.A. BARTOLOTTA and D.L. KRAUSE, Titanium aluminide applications in the High Speed Civil Transport (HSCT), [in:] Y-W. Kim, D.M. Dimiduk, M.H. Loretto [eds.], *Gamma Titanium Aluminides 1999*, TMS, Warrendale, PA, pp.3-10, 1999.

7. R. LEHOLM, H. Clemens, H. Kestler, Powder Metallurgy (PM) gamma-based titanium aluminide structures for use in various high temperature aerospace, [in:] Y-W. Kim, D.M. Dimiduk, M.H. Loretto [eds.], *Gamma Titanium Aluminides 1999*, TMS, Warrendale, PA, pp.25-33, 1999.

8. T. TETSUI, The effect of composition on the endurance of TiAl alloys in turbo-charger application, [in:] Y.-W. Kim, D.M. Dimiduk, M.H. Loretto [eds.], *Gamma Titanium Aluminides 1999*, TMS, Warrendale, PA, pp.15-23, 1999.

9. M. BLUM, A. CHOUDHURY, H. SCHOLZ, G. JARCZYK, S. PLEIER, P. BUSSE, G. FROMMEYER and S. KNIPPSCHEER, Properties of low cost TiAl automotive valves produced by cold wall induction melting and permanent mold centrifugal casting, [in:] Y.-W. Kim, D.M. Dimiduk, M.H. Loretto [eds.], *Gamma Titanium Aluminides 1999*, TMS, Warrendale, PA, pp.35-39, 1999.

10. H. CLEMENS, H. Kestler, Processing and application of intermetallic γ-TiAl-based alloys, *Adv. Eng. Mater.*, Vol.2, pp.551-570, 2000.

11. S. KNIPPSCHEER and G. FROMMEYER, Intermetallic TiAl(Cr,Mo,Si) alloys for lightweight engine parts, *Adv. Eng. Mater.*, Vol.1, pp.187-191, 1999.

12. U.R. KATTNER, J.-C. Lin, Y.A. Chang, Thermodynamic assessment and calculation of the TiAl system, *Met. Trans. A*, Vol.23A, pp.2081-2090, 1992.

13. E.L. HALL and S.C. HUANG, Deformation mechanisms in gamma titanium aluminides. A review, [in:] Y.-W. Kim, R.R. Boyer [eds.], *Microstructure/Property Relationships in Titanium Alumindes and Alloys*, TMS, Warrendale, PA, pp.47-64, 1991.

14. F. APPEL and R. WAGNER, Microstructure and deformation of two-phase γ-titanium aluminides, *Mater. Sci. Eng.*, Vol.R22, pp.187-263, 1998.

15. A. CHATTERJEE, G. DEHM, C. SCHEU and H. CLEMENS, Onset of microstructural instability in a fully lamellar Ti-46.5at%Al-4at%(Cr,Nb,Ta,B) alloy during short term creep, *Z. Metallkd.*, Vol.91, pp.755-760, 2000.

16. M.B. BRADY, W.J. BRINDLEY, J.L. SMIALEK and I.E. LOCCI, The oxidation and protection of gamma titanium aluminides, *JOM*, Vol.11, pp.46-50, 1996

17. F. APPEL, U. Lorenz, J.D.H. Paul, M. Oehring, The Mechanical Properties of Niobium Alloyed Gamma Titanium Aluminides. [in:] Y.-W. Kim, D.M. Dimiduk, M.H. Loretto [eds.], *Gamma Titanium Aluminides 1999*, TMS, Warrendale, PA, pp.381-388, 1999a.

18. F. APPEL, M. OEHRING and P.J. ENNIS, Micromechanisms of creep in gamma-base titanium aluminides, [in:] Y.-W. Kim, D.M. Dimiduk, M.H. Loretto [eds.], *Gamma Titanium Aluminides 1999*, TMS, Warrendale, PA, pp.603-618, 1999b.

19. H. CLEMENS, H. KESTLER, N. EBERHARDT and W. KNABL, Processing of γ-TiAl based alloys on an industrial scale. [in:] Y.-W. Kim, D.M. Dimiduk, M.H. Loretto [eds.], *Gamma Titanium Aluminides 1999*, TMS, Warrendale, PA, pp.209-223, 1999.

20. M. YAMAGUCHI and Y. UMAKOSHI, The deformation behaviour of intermetallic superlattice compounds, *Prog. Mater. Sci.*, Vol.34, pp.1-148, 1990.

21. D. SHECHTMAN, M.J. BLACKBURN and H.A. LIPSITT, The plastic deformation of TiAl, *Metall. Trans.*, Vol.5, pp.1373-1382, 1974.

22. S.L.M. SASTRY and H.A. LIPSITT, Fatigue deformation of TiAl base alloys, *Metall. Trans.*, Vol.8A, pp.299-308, 1977.

23. H. INUI, A. NAKAMURA, M.H. OH and M. YAMAGUCHI, Deformation structures in Ti-rich TiAl polysythetically twinned crystals, *Phil. Mag.*, Vol.A 66, pp.557-573, 1992.

24. Y. UMAKOSHI, T. NAKANO, K. SUMIMOTO and Y. MAEDA, Plastic anisotropiy of Ti_3Al single crystals, *Mater. Res. Soc. Symp. Proc.*, Vol.228, pp.441-446, 1993.

25. R. HILL, Generalized constitutive relations for incremental deformation of metals crystals by multislip, *J. Mech. Phys. of Solids*, Vol.14, pp.95-102, 1966.

26. R. HILL and J.R. RICE, Constitutive analysis of elastic plastic crystals at arbitrary strain, *J. Mech. Phys. of Solids*, Vol.20, pp.401-413, 1972.

27. R. HILL and J.R. RICE, Strain localization in ductile single crystals, *J. Mech. Phys. of Solids*, Vol.25, pp.309-338, 1977.

28. R.J. ASARO, Micromechanics of Crystals and Polycrystals, [in:] J.W. Hutchinson and T.Y. Wu [eds.], *Advances in Applied Mechanics*, Vol.23, pp.1-115, Academic Press, New York 1983.

29. D. PEIRCE, R.J. Asaro, A. Needleman, Material rate dependence and localized deformation in crystalline solids, *Acta metall.*, Vol.31, pp.1951-1976, 1983.

30. R.J. ASARO and A. NEEDLEMAN, Texture development and strain hardening in rate dependent polycrystals, *Acta metall.*, Vol.33, pp.923-953, 1985.

31. A.S. KHAN and S. HUANG, *Continuum Theory of Plasticity*, John Wiley & Sons, pp.29, New York 1995.

32. B.K. KAD, M. DAO and R.J. ASARO, Numerical simulations of plastic deformation and fracture effects in two phase γ-TiAl + α_2-Ti_3Al lamellar microstructures, *Phil. Mag. A*, Vol.71, pp.567-604, 1995.

33. D. PEIRCE R.J. ASARO and A. NEEDLEMAN, An analysis of nonuniform and localized deformation in ductile single crystals, *Acta metall.*, Vol.30, pp.1087-1119, 1982.

34. F. APPEL, An Electron Microscopy Study of Twin Propagation in Two-Phase Titanium Aluminides, [in:] S. Ankem, C.S. Pande [eds.], *Advances in Twinning*, pp.171-186 TMS, Warrendale, PA, 1999.

35. W.F. HOSFORD, *The Mechanics of Crystals and Textured Polycrystals*, pp.163-185, Oxford University Press, New York – Oxford 1993.

36. S.M. SCHLÖGL and F.D. FISCHER, The role of slip and twinning in the deformation behaviour of Polysynthetically Twinned (PST) crystals of TiAl. A micromechanical model, *Phil. Mag. A*, Vol.75, pp.621-636, 1997.

37. J.W. CHRISTIAN and S. MAHAJAN, Deformation twinning, *Prog. Mater. Sci.*, Vol.39, pp.1-157, 1995.

38. A. STAROSELSKY and L. ANAND, Inelastic deformation of polycrystalline face centred cubic materials by slip and twinning, *J. Mech. Phys. of Solids*, Vol.46, pp.671-696, 1998.

39. S.R. KALIDINDI, Incorporation of deformation twinning in crystal plasticity models, *J. Mech. Phys. of Solids*, Vol.46, pp.267-290, 1998.

40. A.R. SRINIVASA, K.R. RAJAGOPAL and R.W. ARMSTRONG, A phenomenological model of twinning based on dual reference structures, *Acta mater.*, Vol.46, pp.1235-1248, 1998.

41. J.K. LEE and M.N. YOO, Elastic strain energy of deformation twinning in tetragonal crystals, *Metal. Trans. A*, Vol.21A, pp.2521-2530, 1990.

42. C.R. HEIPLE and S.H. CARPENTER, Acoustic emission by deformation of metals and alloys – a review, *J. Acoust. Emiss.*, Vol.6, pp.177-204, 1987.

43. S.M. SCHLÖGL, Micromechanical modelling of the deformation behaviour of gamma titanium aluminides, *Fortschrittberichte VDI*, Reihe 18, Nr.220, VDI Verlag, Düsseldorf 1997.

44. T. BIDLINGMAIER, A. WANNER, G. DEHM and H. CLEMENS, Acoustic emission during room temperature deformation of a γ-TiAl based alloy, *Z. Metallkd.*, Vol.90, pp.581-587, 1999.

45. M.H. YOO, C.L. FU and J.K. LEE, The role of twinning in brittle fracture of Ti-aluminides, *Mater. Res. Soc. Symp. Proc.*, Vol.213, pp.545-554, 1991.

46. M.H. YOO, C.L. FU and J.K. LEE, Mechanistic modelling of deformation and fracture behavior in TiAl and Ti_3Al, *Mater. Sci. Eng. A*, Vol.192/193, pp.14-23, 1995.

47. Y. UMAKOSHI, T. NAKANO, K. SUMIMOTO and Y. MAEDA, The role of ordered domains and slip mode of α_2 phase in the plastic behaviour of TiAl crystals containing oriented lamellae, *Acta Metall. Mater.*, Vol.41, pp.1155-1161, 1993.

48. Y. HUANG, *A User-Material Subroutine Incorporating Single Crystal Plasticity in the ABAQUS Finite Element Program*, Report MECH-178, Havard Univ. Rep., 1991.

49. *ABAQUS Finite Element Analysis Products*, Hibbit, Karlsson & Sorensen Inc., (`www.hks.com`).

50. R.E. SCHAFRIK, Dynamic elastic moduli of the titanium aluminides, *Metall. Trans. A*, Vol.8, pp.1003-1006, 1977.

51. M.G. MENDIRATTA, Y.-W. KIM and D.M. DIMIDUK, Loading rate effects and fracture in a TiAl alloy, *Mater. Res. Soc. Symp. Proc.*, Vol.288, pp.543-548, 1993.

52. W.T. MARKETZ, F.D. FISCHER and H. CLEMENS, Micromechanical modelling of the deformation behaviour of gamma titanium aluminides, *Z. Metallkd.*, Vol.90, pp.588-593, 1999.

53. F. KAUFFMANN, T. BIDLINGMAIER, G. DEHM, A. WANNER and H. CLEMENS, On the origin of acoustic emission during room temperature compressive deformation of a γ-TiAl based alloy, *Intermetallics*, Vol.8, pp.823-830, 2000.

54. F. KAUFFMANN, *Schallemission bei der Raumtemperatur-Druckverformung einer γ-TiAl Basislegierung*, Diploma Thesis, University of Stuttgart, 1999.

55. R.E. REED-HILL and R. ABBASCHIAN, *Physical Metallurgy Principles*, PWS Publishing Company, Boston, pp.556-559, 1994.

56. M.A. HAMSTAD, Energy measurement of continuos acoustic emission, [in:] R.K. Miller and P. McIntire [eds.], *NDT Handbook, Section 16: Special Acoustic Emission Applications*, Vol.5, pp.586-591, ASNT, Columbus, OH, 1987.

57. W.T. MARKETZ, F.D. FISCHER, F. KAUFFMANN, G. DEHM, T. BIDLINGMAIER, A. WANNER and H. CLEMENS, On the role of twinning during room temperature deformation of gamma-TiAl based alloys, [in:] *Proc. 3rd Int. Symp. Struct. Func. Intermetallics*, Vancouver 2001a [in press].

58. C.R. HEIPLE and S.S. CHRISTIANSEN, Acoustic emission produced by the deformation of uranium, *J. Acoust. Emiss.*, pp.85-93, 1986.

59. W.T. MARKETZ, F.D. FISCHER, F. KAUFFMANN, G. DEHM, T. BIDLINGMAIER, A. WANNER and H. CLEMENS, Computational modeling and experimental study of the deformation behavior of γ-TiAl based alloys, *Adv. Eng. Mater.*, Vol.2, pp.662-666, 2000.

60. T.A. PARTHASARATHY, M. KELLER and M.G. MENDIRATTA, The effect of lamellar lath spacing on the creep behavior of Ti-47at%Al, *Scripta Mater.*, Vol.37, pp.1025-1031, 1998.

61. P.D. CROFTS, P. BOWEN and I.P. JONES, The effect of lamella thickness on the creep behaviour of Ti-48Al-1Nb-2Mn, *Scripta Mater.*, Vol.35, pp.1391-1396, 1996.

62. K. MARUYAMA, R. YAMAMOTO, H. NAKAKUKI and N. FUJITSUNA, Effects of lamellar spacing, volume fraction and grain size on the creep strength of fully lamellar TiAl alloys, *Mater. Sci. Eng.*, Vol.A239-240, pp.419-428, 1997.

63. W.T. MARKETZ, A. CHATTERJEE, F.D. FISCHER and H. CLEMENS, Creep of γ-TiAl based alloys. Experiments, computational modelling. [in:] S. Murakami and N. Ohno [eds.], *Solid Mechanics and its Applications*, Vol.86, IUTAM Symposium on Creep in Structures, pp.17-30, Kluwer Academic Publishers, Dordrecht 2001b.

64. H. INUI, M.H., OH, A. NAKAMURA and M. YAMAGUCHI, Ordered domains in TiAl coexisting with Ti_3Al in the lamellar structure of Ti-Rich TiAl compounds, *Phil. Mag. A*, Vol.66, pp.539-555, 1992.

65. T. FUJIWARA, A. NAKAMURA, M. HOSOMI, S.R. NISHITANI, Y. SHIRAI and M. YAMAGUCHI, Deformation of polysynthetically twinned crystals of TiAl with nearly stoichiometric composition, *Phil. Mag. A*, Vol.61, pp.591-606, 1990.

66. H. CLEMENS, W. GLATZ, N. EBERHARDT, H.P. MARTINZ and W. KNABL, Processing, properties and application of gamma titanium aluminide sheet and foil materials, *Mater. Res. Soc. Symp. Proc.*, Vol.460, pp.29-43, 1997.

67. A. CHATTERJEE, U. BOLAY, U., SATTLER and H. CLEMENS, Adjustment of differently spaced fully lamellar microstructures in a γ-TiAl based alloy and their creep behavior, [in:] *Intermetallics and Superalloys EUROMAT 10*, Wiley-VCH, Weinheim, pp.233-239, 2000.

68. J.N. WANG, A.J. SCHWARTZ, T.G. NIEH, C.T. LIU, V.K. SIKKA and D. CLEMENS, Creep of a Fine Grained, Fully Lamellar, Two Phase TiAl Alloy at 760°. [in:] Y.-W. Kim, R. Wagner and M. Yamaguchi [eds.], *Gamma Titanium Aluminides*, TMS, Warrendale, PA, pp.949-957, 1995.

69. W.R. CHEN, J. TRIANTAFILLOU, J. BEDDOES and L. ZHAO, Effect of fully lamellar morphology on creep of a near gamma TiAl intermetallic, *Intermetallics*, Vol.7, pp.171-178, 1999.

70. M.F. BARTHOLOMEUSZ, Q. YANG and J.A. WERT, Creep deformation of a two-phase TiAl/Ti_3Al lamellar alloy and the individual TiAl and Ti_3Al constituent phases, *Scripta Met.Mater.*, Vol.29, pp.389-394, 1993.

71. G. WEGMANN, T. SUDA and K. MARUYAMA, Creep deformation of Polysynthetically Twinned (PST) Ti-48mol%Al, *Key Engineering Materials*, Vol.170-174, pp.709-716, 2000.

72. H. INUI, K. KISHIDA, M. MISAKI, M. KOBAYASHI, Y. SHIRAI and M. YAMAGUCHI, Temperature dependence of yield stress, tensile elongation and deformation structures in polysynthetically twinned crystals of Ti-Al, *Phil. Mag. A*, Vol.72, pp.1609-1631, 1995.

73. M. ES-SOUNI, A. BARTELS and R. WAGNER, Creep behaviour of a near γ-TiAl alloy Ti-48Al-2Cr. Effect of microstructure, [in:] R. Darolia, J.J.Lewandowski, C.T. Liu, P.L. Martin, D.B. Miracle and M.V. Nathal [eds.], *Structural Intermetallics*, pp.335-343, TMS, Warrendale, PA, 1993.

74. Y. HE, R.B. SCHWARZ, T. DARLING, M. HUNDLEY, S.H. WHANG and Z.M. WANG, Elastic constants and thermal expansion of single crystal γ-TiAl from 300 to 750 K, *Mater. Sci. Eng. A*, Vol.239-240, pp.157-163, 1997.

75. H. PETRYK, Material instability and strain rate discontinuities in incrementally non-linear continua, *J. Mech. Phys. of Solids*, Vol.40, pp.1227-1250, 1992.